The Effect of Dynamics on Mixed-Phase Clouds: Theoretical Considerations

ALEXEI KOROLEV

Environment Canada, Toronto, Ontario, Canada

PAUL R. FIELD

National Center for Atmospheric Research, Boulder, Colorado

(Manuscript received 21 November 2006, in final form 26 February 2007)

ABSTRACT

A theoretical framework has been developed describing nonequilibrium formation and maintenance of mixed-phase clouds. The necessary and sufficient conditions required to activate liquid water within a preexisting ice cloud, and thus convert it to mixed phase, are considered for three scenarios: (i) uniform ascent, (ii) harmonic vertical oscillations, and (iii) turbulent fluctuations. The general conditions are the following:

1) First necessary condition: The vertical velocity of an ice cloud parcel must exceed a threshold velocity to activate liquid water.
2) Second necessary condition: The activation of liquid water within an ice cloud parcel, below water saturation, requires a vertical ascent above some threshold altitude to bring the vapor pressure of the parcel to water saturation.

Only when the first *and* second conditions are true do these conditions become sufficient for the activation of liquid water in ice clouds. These required conditions for the generation of mixed-phase cloud are supported by parcel modeling results and analogous conditions for a harmonic oscillation concerning the amplitude and tangential velocity of the parcel motion are proposed. The authors do not assume steady-state conditions, but demonstrate that nonequilibrium evolution of cloud parcels can lead to long-term steady existence of mixed-phase cloud.

1. Introduction

Mixed-phase clouds are notoriously difficult to represent in numerical weather prediction and climate models (e.g., Illingworth et al. 2007). This shortcoming has consequences ranging from the success of operational prediction of in-cloud icing for aviation to the longevity and areal extent of supercooled-layer clouds that can have an impact on the radiative balance of the atmosphere important for climate prediction. Proper simulation of mixed-phase clouds is also essential in precipitation modeling, which impacts the hydrological cycle. Mixed-phase clouds are difficult to represent in large-scale models because the temporal and spatial scales of this phenomenon are typically smaller than the model grid spacing employed. Representation of "subgrid" processes can be successful if sufficient physical understanding of the phenomenon can be embedded in the model.

The Wegener–Bergeron–Findeisen (WBF) mechanism (Wegener 1911; Bergeron 1935; Findeisen 1938) describes the process by which water is repartitioned when liquid droplets, ice crystals, and water vapor are all well mixed and not subject to any mean changes in temperature and/or pressure. Such a combination is unstable and because the saturated water vapor pressure over water is greater than that over ice at the same temperature, the ice crystals will grow at the liquid droplets expense. Eventually, the liquid droplets will completely evaporate and the water will reside in the vapor and ice phases only.

Previous theoretical studies have suggested that the glaciation of mixed-phase clouds with ice particle concentrations $N_i \sim 10^2$–10^3 L^{-1} and liquid water content below 0.5 g m^{-3} should occur within 20–40 min (e.g., Korolev and Isaac 2003). However, in situ observations have shown that mixed-phase clouds are a common

Corresponding author address: Alexei Korolev, Environment Canada, 4905 Dufferin Street, Toronto, ON M3H 5T4, Canada.
E-mail: alexei.korolev@ec.gc.ca

DOI: 10.1175/2007JAS2355.1

phenomenon (e.g., Borovikov et al. 1963; Korolev et al. 2003; Verlinde et al. 2007). Rauber and Tokay (1991) and Pinto (1998) have described long-lived narrow layers of supercooled water overlying mixed and ice layers with cloud tops as cold as −30°C. The existence of such layers appears to conflict with the outcome expected from the WBF mechanism. Rauber and Tokay (1991), Pinto (1998), Harrington et al. (1999), and Harrington and Olsson (2001) attempted to explain the existence of such layers by an imbalance between the condensate supply rate, the bulk ice crystal mass growth rate, and removal of ice freezing nuclei (IFN) by precipitating ice particles. Field et al. (2004) suggested that observations of embedded liquid water regions with horizontal extents as short as 100 m may be the result of turbulent motions leading to the intermittent production of liquid water. Korolev and Isaac (2003) found that a cloud parcel undergoing vertical oscillations may be subject to an indefinitely long periodic evaporation and activation of liquid droplets in the presence of ice particles. After a certain amount of time, the average ice water content (IWC) and LWC reaches a steady state. This phenomenon may explain the existence of long-lived mixed-phase stratiform layers.

While it has long been recognized that the WBF mechanism is a major process in precipitation formation in cold clouds, most theoretical efforts have focused on studies of the transition of mixed phase into ice clouds. Heymsfield (1977) was the first to recognize that ice clouds could be turned into mixed phase through the activation of liquid water in updrafts. Since then a few studies have investigated the minimum updraft required to maintain steady-state mixed-phase conditions (e.g., Mazin 1986; Tremblay et al. 1996; Zawadzki et al. 2000).

The intention of this paper is to continue the theoretical considerations of the generation maintenance and decay of ideal mixed-phase clouds (Mazin 1986; Korolev and Isaac 2003; Korolev and Mazin 2003) under nonsteady-state conditions in order to provide both qualitative and quantitative understanding of mixed-phase cloud at small scales (subkilometer) upon which future parameterizations may be based.

2. Necessary and sufficient conditions for activation of liquid in ice cloud

In this section we outline the conditions required to create a mixed-phase cloud. A number of simplifying assumptions have been made: (i) liquid and ice size distributions are monodisperse; (ii) ice particles are spherical; (iii) the microphysical details of ice nucleation and droplet nucleation are neglected: seed liquid droplet and ice crystal number and size are specified; (iv) sedimentation is ignored; (v) ventilation effects on growth are ignored; (vi) aggregation of ice crystals and coalescence of droplets is ignored; (vii) riming is ignored; (viii) the cloud parcel is homogeneous, isotropic, adiabatic, and mixing is ignored; (ix) radiation effects are ignored. It is recognized that these simplifications will mean that some of the quantitative results will not be directly applicable to real cloud systems and this will be addressed in the discussion. However, such simplifications allow us to build a good theoretical understanding of mixed-phase phenomena that will aid us when attempting to construct a parameterization with more realistic assumptions included. The effect of the simplifications stated above will be considered in more details in section 6.

We will first identify the conditions required for converting an ice-only cloud parcel into one containing both ice and liquid.

a. First necessary condition

The first necessary condition is that the vertical velocity of an ice cloud parcel must exceed a threshold velocity to activate liquid water.

As remarked in the introduction, various authors have considered the updraft necessary to maintain mixed-phase conditions for steady-state conditions. Similarly, through consideration of the quasi-steady relative humidity of a cloud parcel, Korolev and Mazin (2003) found a threshold vertical velocity

$$u_z^* = \frac{B_i^* N_i \bar{r}_i}{a_w} \tag{1}$$

that must be exceeded to activate liquid water in ice clouds, that is

$$u_z > u_z^*, \tag{2}$$

where N_i, $\bar{r}_i$ are the concentration and average size of ice particles, and a_w, B_i^* are coefficients dependent upon T and p (an explanation of all the variables used in the text is provided in appendix A).

Figure 1 shows the dependence of the threshold velocity upon ice particle integral radius $N_i\bar{r}_i$ (first moment of the size distribution). Figure 1 shows that for typical values of $N_i\bar{r}_i$ (gray area) the threshold velocity u_z^* changes from a few centimeters to a few meters per second over a wide range of temperatures and pressures. In situ observations show that such vertical velocities are common in clouds and can be generated by turbulence or regular motions (e.g., convection or gravity waves). Therefore, Fig. 1 suggests that mixed-phase clouds can be formed in the atmosphere through the

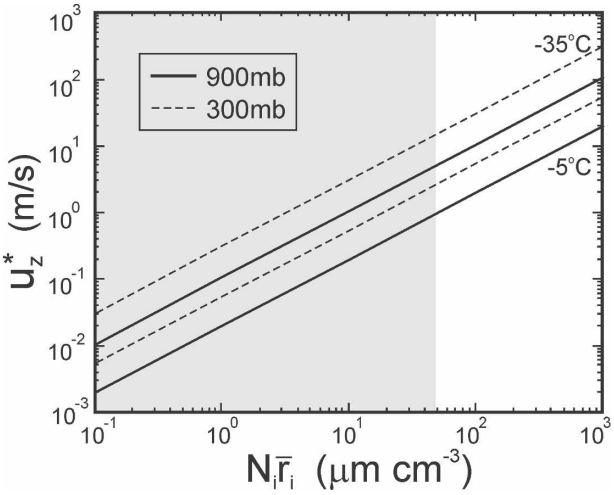

FIG. 1. Threshold velocity of ascent required for activation of liquid in ice cloud vs the integral radii of ice particles for different temperatures and pressures at $RH_w = 100\%$ for two temperatures: −5°C (two lower lines) and −35°C (two upper lines). Gray area indicates $N_i\bar{r}_i$ typically observed in ice clouds.

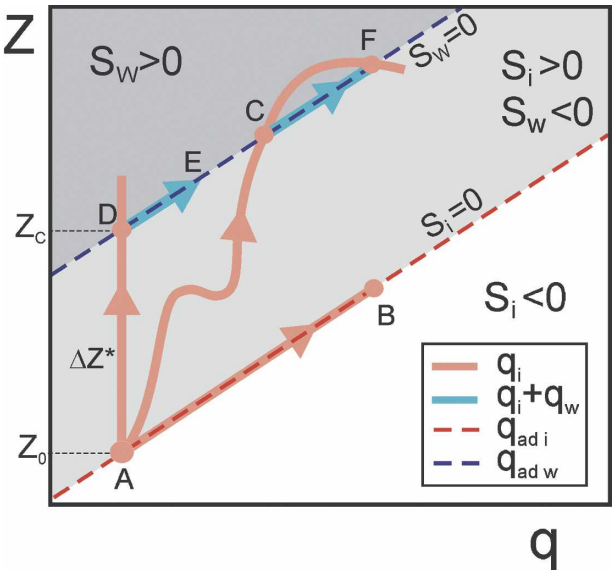

FIG. 2. Conceptual diagram of the activation of liquid phase in an ascending parcel within an ice cloud. Activation of liquid phase occurs when a trajectory $q_{ice}[z(t)]$ intersects $q_{ad\ w}(z)$ (e.g., points C and D). The dark gray area above the liquid water adiabat $q_{ad\ w}(z)$ is supersaturated with respect to water ($S_w > 0$), the area below the ice water adiabat $q_{ad\ i}(z)$ is subsaturated with respect to ice ($S_i < 0$), and the light gray area between $q_{ad\ w}(z)$ and $q_{ad\ i}(z)$ is supersaturated with respect to ice and subsaturated with respect to water ($S_i > 0$ and $S_w < 0$).

activation of liquid water within preexisting ice clouds. The first condition provides the necessary but not sufficient condition for the activation of the liquid phase within ice clouds. For example, the condition in Eq. (2) may be satisfied even though the water vapor pressure is lower than its saturation value over water. In this case, the activation of liquid water will not occur and the cloud will remain in the ice phase. Such a consideration automatically leads to the second condition.

b. Second necessary condition

The activation of liquid water within an ice cloud parcel, below water saturation, requires a vertical ascent (ΔZ) above some threshold altitude (ΔZ^*) to bring the vapor pressure of the parcel to water saturation:

$$\Delta Z > \Delta Z^*. \tag{3}$$

Only when the first *and* second conditions are true do these conditions become sufficient for the activation of liquid water in ice clouds.

To examine the processes of activation, condensation, and evaporation of liquid droplets in presence of ice particles, we consider the changes of cloud water mixing ratio in the Q–Z (condensed water–height) coordinates (Fig. 2). For simplicity, we assume that the initial relative humidity inside the cloud parcel is equal to ice saturation (point A in Fig. 2), and that the ice particles are in equilibrium with water vapor. If the ascent velocity of the parcel is infinitely small ($u_z \to 0$), then the ice particles have enough time to accommodate water vapor supersaturation caused by adiabatic cooling during ascent, and the ice water mixing ratio (q_i) will change along an ice adiabat (line AB in Fig. 2). The relative humidity inside this parcel will always be at ice saturation, and it will never reach water saturation. If the velocity of ascent is infinitely large ($u_z \to \infty$), then the vertical gradient of ice water mixing ratio will be infinitely small; that is, $dq_i/dz \to 0$ and q_i will be constant (see appendix B). In this case, the relative humidity in the parcel will change as if it were in a cloud-free volume (appendix C):

$$\frac{1}{S_w + 1}\frac{dS_w}{dz} = a_w. \tag{4}$$

Here, $S_w = e/E_w - 1$ is the water vapor supersaturation over a liquid surface, e is water vapor pressure, $E_w(T)$ is saturated vapor pressure over liquid water at temperature T, and a_w is a coefficient dependent on temperature.

Integrating Eq. (4) yields the vertical distance required for an adiabatic parcel to ascend from the level having initial vapor pressure e_0 up to a level at water saturation E_w (line AD in Fig. 2):

$$\Delta Z_c = a_w^{-1} \ln\left(\frac{E_w}{e_0}\right). \tag{5}$$

The value of ΔZ_c gives the minimum vertical distance for a parcel within an ice cloud to achieve saturation over water; that is,

$$\Delta Z^*_{\min} = \Delta Z_c. \tag{6}$$

Figure 3 shows the dependence of ΔZ_c on temperature for three different initial humidities. As seen from Fig. 3, ΔZ_c monotonically decreases with an increase of temperature. For $e_0 = E_i$ and $T > -20$°C, ΔZ_c does not exceed 300 m. Since we expect the occurrence of fluctuations with smaller vertical displacements, ΔZ, to be greater than those with larger vertical displacements, it may be reasonable to think that the probability of formation of mixed-phase clouds at warmer temperatures is higher than that at low temperatures through inspection of Fig. 3.

Returning to Fig. 2, if the *first necessary condition* [Eq. (2)] is satisfied, then the ascent of a cloud parcel beyond the point D [*second necessary condition*, Eq. (3)] will result in the condensation of liquid water and the ice cloud will become mixed phase. Assuming that the sink of water vapor supersaturation to liquid droplets is instantaneous, the total condensed cloud water mixing ratio in the cloud ascending above the point D (line DE in Fig. 2) with the vertical speed $u_z > u_z^*$ will be equal to the adiabatic liquid water $[q_{\text{ad }w}(z)]$ passing through point D; that is,

$$q_i(z) + q_w(z) = q_{\text{ad }w}(z). \tag{7}$$

The adiabatic liquid ($q_{\text{ad }w}$) and ice ($q_{\text{ad }i}$) water mixing ratios are defined by initial ice water mixing ratio, q_{i0}, relative humidity and temperature, and they can be found (appendix D) using

$$q_{\text{ad }w}(z) = (q_{i0} + \delta q_i) + \int_{z_0+\Delta Z_c}^{z} \beta_w(z')\,dz', \tag{8}$$

$$q_{\text{ad }i}(z) = (q_{i0} + \delta q_i) + \int_{z_0}^{z} \beta_i(z')\,dz', \tag{9}$$

where β_w and β_i are the adiabatic vertical gradients of liquid and ice water mixing ratio, respectively; q_{i0} is the initial ice water mixing ratio of the parcel; and δq_i is an offset applied to the adiabatic ice water mixing ratio to account for initial sub- or supersaturation with respect to ice (see appendix D). The sum $(q_{i0} + \delta q_i)$ is the adiabatic ice water mixing ratio at z_0. In Fig. 2 the initial conditions at point A are such that $\delta q_i = 0$.

At the beginning of this section we considered two extreme cases for the ideal ice clouds ascending with infinitely small and infinitely large vertical velocities. In real clouds the limited rate of condensation and evaporation of cloud particles will lead to $q_i[z(t)]$ trajectories that will lie somewhere between the two extreme cases;

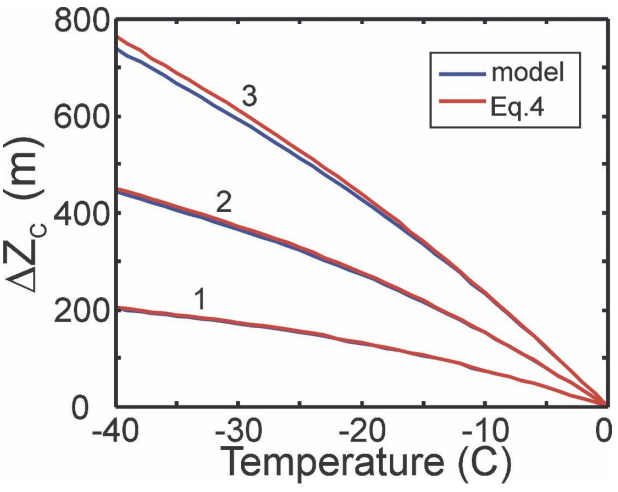

FIG. 3. Vertical distance required for reaching saturation over water in the adiabatically ascending parcel vs temperature calculated from Eq. (5) and derived from numerical model (for details see appendixes C and F). Initial humidity in the parcel: 1) $e_0 = E_i + (E_w - E_i/2)$ (supersaturation with respect to ice, midpoint between saturation over ice and liquid), 2) $e_0 = E_i$ (ice saturation), and 3) $e_0 = E_i - (E_w - E_i/2)$ (subsaturation with respect to ice).

that is, $q_i[z(t)]$ will be between lines AB and AD in Fig. 2 and will be a solution of the following equation describing the change of q_i when the parcel is in the ice phase only (appendix E):

$$\frac{d^2q_i}{dt^2} - \left(\frac{1}{3q_i} + b_i\right)\left(\frac{dq_i}{dt}\right)^2 + (\vartheta q_i^{1/3} - a_i u_z)\frac{dq_i}{dt} - \chi u_z q_i^{1/3} = 0. \tag{10}$$

Because a_i, b_i, ϑ, and χ are coefficients dependent upon T and P (appendix A) the solution for q_i will be a function of vertical velocity:

$$q_i[z(t)] = F[u_z(t)]. \tag{11}$$

This formulation of $q_i(t)$ enables a general conclusion to be drawn about the existence of an ensemble of trajectories $u_z(t)$ that result in an intersection of $q_i[z(t)]$ and $q_{\text{ad }w}(z)$. The proof of this statement is presented in appendix B. That is to say that the activation of the liquid phase in ascending adiabatic parcels within ice clouds will occur only if the system of Eqs. (8) and (11) has a solution: $q_i(z) = q_{\text{ad }w}(z)$. This solution of Eq. (8) and (11) satisfies both of the necessary conditions stated above.

The condition for the activation of liquid water within ice clouds has a simple graphical interpretation: the activation of liquid water occurs in an ascending *ice cloud* parcel when the curve $q_i[z(t)]$ intersects $q_{\text{ad }w}(z)$ in Q–Z coordinates (point C in Fig. 2). If the intersection of $q_i[z(t)]$ and $q_{\text{ad }w}(z)$ occurs when the parcel is

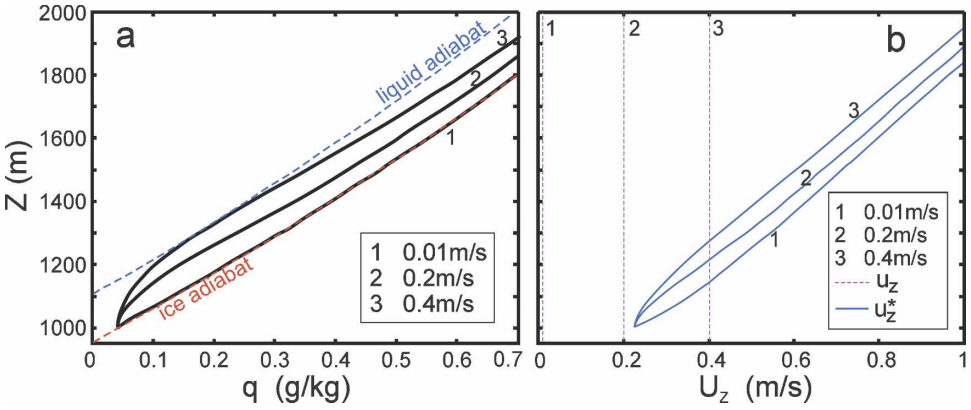

FIG. 4. Numerical modeling of ice water mixing ratio vs height in a uniformly ascending adiabatic parcel demonstrating that Eq. (2) is a necessary but not sufficient condition for activation of liquid water within ice cloud; $N_i = 100\ \mathrm{L}^{-1}$, $r_{i0} = 50\ \mu\mathrm{m}$, $S_{i0} = 0$, $T = -10°\mathrm{C}$. (a) Vertical changes of ice water mixing ratios; (b) vertical changes of threshold velocity, u_z^*, calculated from Eq. (1) and velocity of the parcel, u_z.

already mixed phase, then it will correspond to the evaporation of droplets and glaciation of the mixed-phase parcel (point F in Fig. 2). It should be noted that the glaciation of mixed-phase clouds can occur both during ascents and descents. Examples of glaciation during ascent and descent will be considered in sections 3 and 4.

In the next three sections we will consider conditions for the formation of mixed-phase clouds during uniform ascent, vertical harmonic oscillations, and turbulent fluctuations.

3. Uniform ascent

This section demonstrates the characteristics of the formation of mixed-phase cloud in a uniformly ascending parcel. Figure 4a shows the modeled changes of ice water mixing ratio within adiabatic parcels uniformly ascending at different u_z. The numerical model of activation and evolution of liquid water and ice within a cloud parcel is described in appendix F. Because the size of the ice particles $\bar{r}_i$ increases during the ascent, then, in accordance with Eq. (1), the threshold velocity, u_z^*, also increases (Fig. 4b). For the slowest ascent $u_z = 0.01\ \mathrm{m\ s}^{-1}$ shown in Fig. 4a (line 1), the change in $q_i(z)$ with height is close to the ice adiabat, $q_{\mathrm{ad}\ i}(z)$. As u_z increases ($u_z = 0.2\ \mathrm{m\ s}^{-1}$, line 2) the deviation of $q_i(z)$ from $q_{\mathrm{ad}\ i}(z)$ increases as well. For $u_z = 0.2\ \mathrm{m\ s}^{-1}$ activation of liquid does not occur, because $u_z < u_z^*$ always (Fig. 4b). The parcel ascending with $u_z = 0.4\ \mathrm{m\ s}^{-1}$ (line 3) initially satisfies the necessary condition that $u_z > u_z^*$ (Fig. 4b). However, as the parcel trajectory reaches the liquid adiabat, the parcel velocity no longer exceeds the threshold velocity and the parcel remains in the ice phase.

Figure 5 shows the modeled activation of liquid water within an ice cloud for a cloud parcel ascending with $u_z = 0.5\ \mathrm{m\ s}^{-1}$. No activation of liquid droplets occurs below the level indicated by line Z_a, even though $u_z > u_z^*$ (line OA in Fig. 5b), since the water vapor pressure has not reached water saturation. The activation of water occurs as soon as $q_i(z)$ intersects the liquid water adiabat $q_{\mathrm{ad}\ w}(z)$ at the level Z_a (Fig. 5a). At this point, both necessary conditions required to activate liquid water within an ice cloud are satisfied. Above the level Z_a total water mixing ratio $q_i(z) + q_w(z)$ (gray line) follows the liquid adiabat $q_{\mathrm{ad}\ w}(z)$ (upper dashed line on Fig. 5a) until it reaches the level Z_e at which the droplets will completely evaporate, $q_i(z)$ will be equal to the liquid adiabat $q_{\mathrm{ad}\ w}(z)$, and the parcel will return to the ice phase. Liquid water mixing ratio $q_w(z)$ reaches a maximum at the level Z_m where $u_z = u_z^*$ (point B in Fig. 5b) and then it starts to evaporate since $u_z < u_z^*$ (Fig. 5b). Once liquid is activated and a mixed-phase cloud is formed, the *maintenance* of mixed phase requires that the $q_i(z)$ trajectory remains above $q_{\mathrm{ad}\ w}(z)$.

Figure 6 shows a conceptual diagram summarizing the effect of vertical velocity on activation of liquid water in ice clouds during uniform ascent. In the previous examples we have seen that even if the ascent velocity of the parcel u_z initially exceeds the threshold velocity u_z^* it may still fall below this threshold during the ascent and prevent the parcel intercepting the liquid adiabat. We can define a minimum ascent velocity ($u_{z\,\mathrm{min}}^*$) that has the property of being equal to the

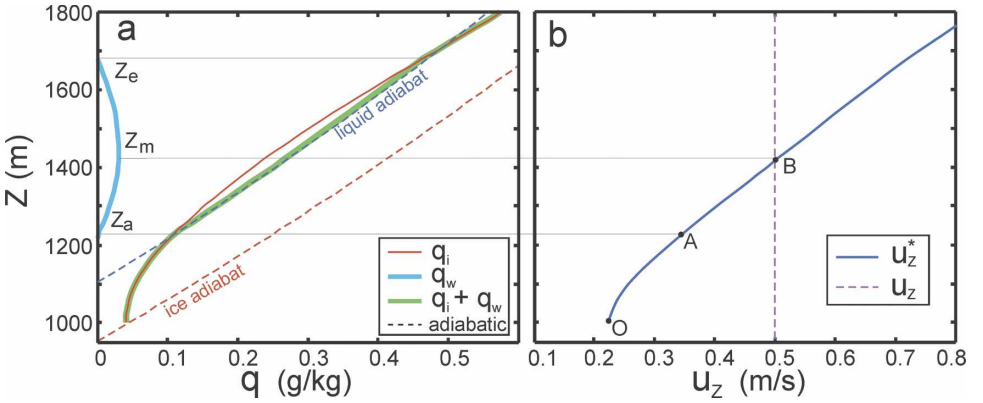

FIG. 5. Numerical modeling of the activation of liquid water within ice cloud in a uniformly ascending adiabatic parcel with $u_z = 0.5$ m s^{-1}, $N_i = 100$ L^{-1}, $r_{i0} = 50$ μm, $S_{i0} = 0$, and $T = -10$°C. (a) Vertical changes of ice, liquid, and total water mixing ratios; (b) vertical changes of threshold velocity [Eq. (1)] and velocity of the parcel.

threshold velocity at the instant the parcel reaches water saturation at a height $Z^*_{\max}$. The velocity $u^*_{z\,\min}$ divides the behavior of uniform ascents into two regimes (Fig. 6b). For ascent velocities $u_z < u^*_{z\,\min}$ activation of the liquid phase is impossible for any z (in Fig. 6b vertical ascents with constant velocities trace vertical trajectories in U–Z space). If $u_z > u^*_{z\,\min}$, the curve $q_i(z)$ intersects $q_{\mathrm{ad}\,i}(z)$ at two points (see also Fig. 5a). The first intersection (Fig. 6b, line 1) occurs at $Z_c < z < Z^*_{\max}$, and it corresponds to activation of liquid water. The second intersection (Fig. 6b line 2) occurs at some altitude $z > Z^*_{\max}$, and it corresponds to evaporation of liquid water and conversion of the mixed-phase cloud into ice only. The evaporation of water occurs since the ice will grow to such an extent that the growth rate of the ice particles will eventually drive the relative humidity of the parcel back below water saturation and return it to the ice phase as the droplets evaporate. At $u_z \to \infty$, the activation of liquid water takes place at $z \to Z_c$, which represents the minimum altitude at which liquid activation can occur.

Figure 7 shows regions of mixed phase in U–Z coordinates for different initial temperatures deduced from numerical simulations. The modeling was performed for $S_{i0} = 0$, $r_{i0} = 50$ μm, and $N_i = 0.1$ cm^{-3}. Comparison between Figs. 7 and 3 indicates that $Z^*_{\max} \approx 2Z_c$, although this will change with initial conditions. Figure 7 indicates that the formation of mixed phase at lower temperatures requires higher vertical excursions and higher velocity as $u^*_{z\,\min}$ and $Z^*_{\max}$ increase. Therefore, it is to be expected that formation of mixed phase at lower temperatures is less probable than formation at higher temperatures.

Thus, summarizing the above we can conclude that

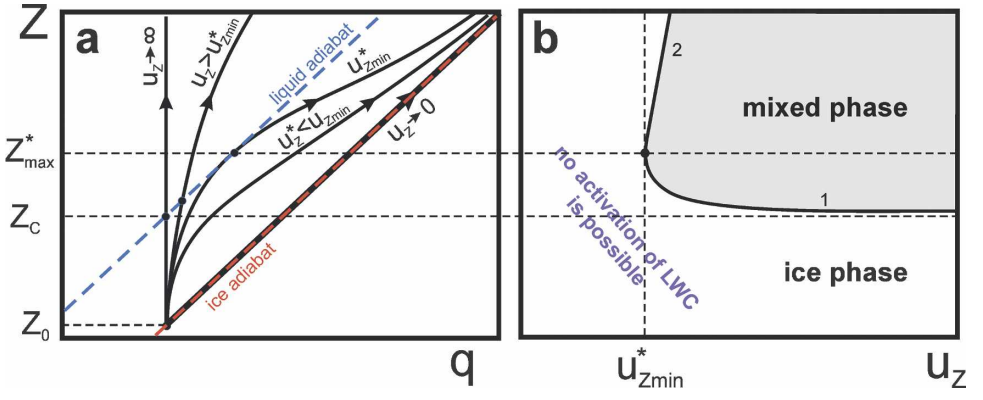

FIG. 6. Conceptual diagrams showing (a) levels at which activation of the liquid phase occurs in a uniformly ascending ice clouds in Q–Z coordinates. (b) Regions of existing ice and mixed-phase clouds in U–Z coordinates. Curve 1 indicates the level at which activation of liquid water occurs in ice cloud and turns it into mixed phase. Curve 2 indicates the level at which evaporation of liquid takes place that turns the mixed-phase cloud into ice.

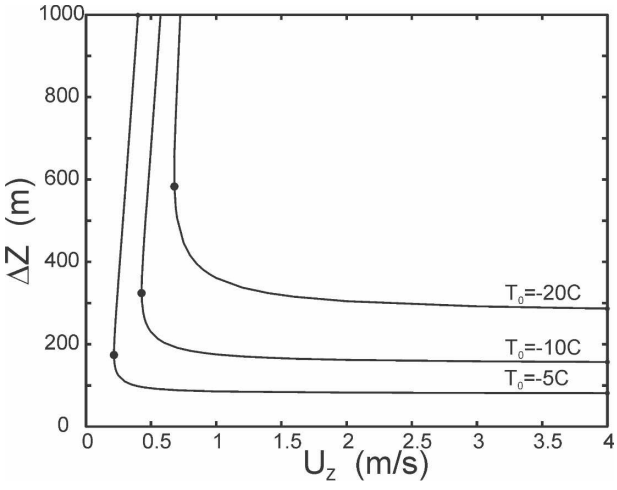

FIG. 7. Curves, separating ice (below) and mixed-phase (above) clouds formed in uniformly ascending parcels for different initial temperatures: −5°, −10°, and −20°C. Solid circles indicate $Z^*_{\max}$. The calculations were conducted for $N_i = 100$ L^{-1}, $r_{i0} = 50$ μm, $S_{i0} = 0$, $H_0 = 1000$ m, and $c = 1$.

for the activation of liquid water in a uniformly ascending ice cloud it is necessary and sufficient that $u_z > u^*_{z\,\min}$, *and* that the altitude of ascent exceeds a threshold altitude $z > Z^*$. As was shown above, for a uniform ascent the threshold altitude Z^* changes in the range $Z_c < Z^* < Z^*_{\max}$, and it is a function of the vertical velocity, that is $Z^*(u_z)$. Whereas the threshold vertical velocity $u^*_{z\,\min}$ is a function of N_i, r_{i0}, N_w, r_{w0}, T, and P.

4. Vertical harmonic oscillations

In general, the system of Eqs. (8) and (11) does not have an analytic solution for arbitrary $u_z(t)$. Thus, in order to predict the formation of mixed-phase clouds, a system of differential equations that describes the cloud microphysics have to be numerically solved. The initial conditions required for satisfying the necessary and sufficient conditions for the activation of liquid water within ice clouds can be found for some special cases. In the following section we discuss the formation of mixed-phase clouds during harmonic oscillations of $u_z(t)$.

a. Ice clouds

Before proceeding with the analysis of the activation of liquid water in a vertically oscillating parcel, we will examine some characteristic features of the condensation–evaporation processes in an ice-only cloud during harmonic oscillations with vertical velocity $u_z = u_0 \sin(\omega t)$, where $\omega = 2\pi/t_0$, $t_0 = \pi\Delta Z/u_0$ is the period of oscillations; ΔZ is the amplitude of oscillations; and u_0 is the tangential velocity. No activation of liquid water is allowed during these oscillations, and the cloud remains in a two-phase condition consisting of ice particles and water vapor.[1]

The supersaturation with respect to ice in the parcel can be presented in a form (e.g., Korolev and Mazin 2003)

$$\frac{dS_i}{dt} = AS_i^2 - BS_i + C. \tag{12}$$

Here A, B, and C are the coefficients dependent upon N_i, r_i, P, and T (appendix A)

Analysis of Eq. (12) suggests that the characteristic time of relaxation to a quasi-steady supersaturation in the ascending parcels is defined by the so-called time of phase relaxation (Mazin 1986; Korolev and Mazin 2003):

$$\tau_{\rm ph} = \frac{1}{B_i N_i \bar{r}_i + a_i u_z}. \tag{13}$$

If the characteristic time of vertical motion

$$\tau_z \gg \tau_{\rm ph}, \tag{14}$$

then ice particles will have enough time to accommodate (release) water vapor during ascents (descents), and bring the two-phase "ice vapor" system into quasi equilibrium. It has been shown that the supersaturation $S_i(t)$ in a cloud parcel approaches a quasi-steady value $S_{{\rm qs}i}(t)$, with time (Korolev and Mazin 2003):

$$\lim_{t\to\infty} S_i(t) = S_{{\rm qs}i}(t). \tag{15}$$

For example, typically over $3\tau_{\rm ph}$ the difference between $S_i(t)$ and $S_{{\rm qs}i}(t)$ becomes smaller than 10%. Since $\lim_{t\to\infty} S_{{\rm qs}i} = 0$ (Sedunov 1974), then $\lim_{t\to\infty} S_i = 0$ as well. Therefore, $\lim_{t\to\infty} q_i = q_{{\rm ad}\,i}$, because $S_i \propto (q_i - q_{{\rm ad}\,i})$. Thus, for characteristic vertical fluctuations with a time scale $\tau_z \gg \tau_{\rm ph}$, the ice water mixing ratio, q_i, approaches its adiabatic value. If the condition in Eq. (14) is not valid then q_i may differ significantly from $q_{{\rm ad}\,i}$, and such cases are important for the activation of liquid water within parcels subjected to vertical harmonic oscillations.

Figure 8 illustrates the different behaviors of q_i in four parcels having the same amplitude of vertical oscillation $\Delta Z = 200$ m, but different velocities $u_0 = 0.02$, 0.2, 1, and 5 m s^{-1}. The initial conditions for all of the parcels were the same: $N_i = 1000$ L^{-1}; $r_{i0} = 20$ μm; $T_0 = -10$°C; and $S_{i0} = 0.01$. Figure 8 indicates that q_i,

[1] The following consideration is also valid for two-phase system consisting of liquid droplets and water vapor.

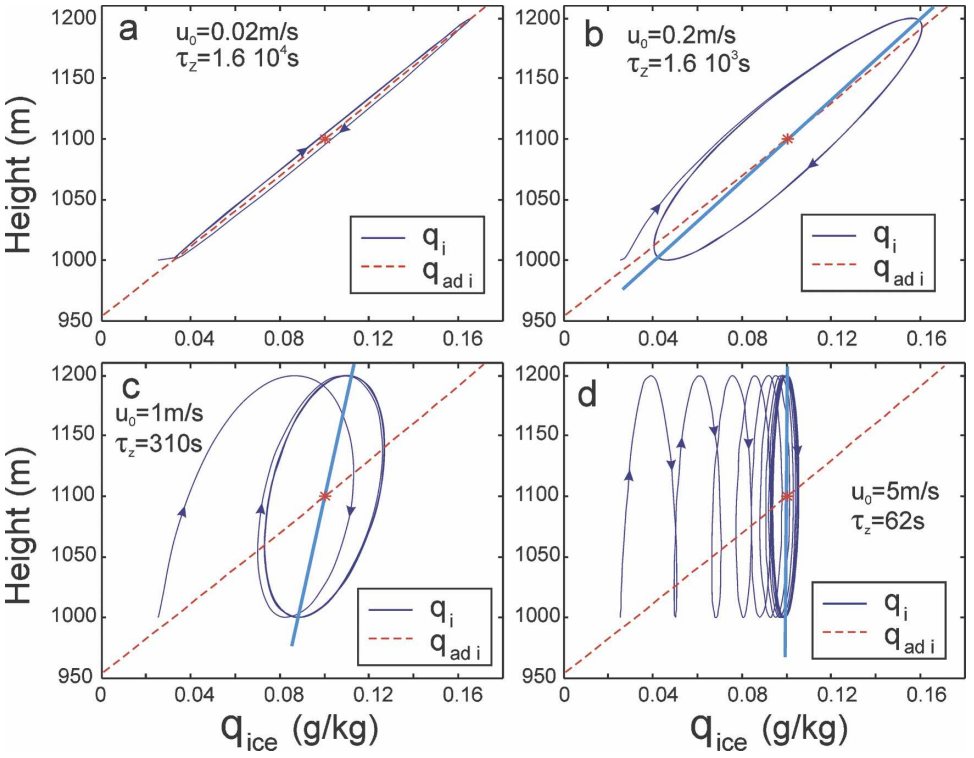

FIG. 8. Changes of ice water mixing ratio in an adiabatic ice cloud when the vertical velocity varies as $u_z = u_0 \sin(\omega t)$. For all four cases $N_i = 1000$ L^{-1}, $r_{i0} = 20$ μm, $\Delta Z = 200$ m, $\tau_{ph} \approx 220$s, $T_0 = -10$°C, and $S_{i0} = 0.01$. (a) Here $\tau_z \gg \tau_{ph}$, $\tau_z \approx 1.6\ 10^4$ s; (b) $\tau_z > \tau_{ph}$, $\tau_z \approx 1.6\ 10^3$ s; (c) $\tau_{ph} \sim \tau_{ph}$, $\tau_z \approx 310$ s; and (d) $\tau_z < \tau_{ph}$, $\tau_z \approx 62$ s. The light blue line indicates the major axis of the limit cycle centered on the red star.

with time, approaches a limit cycle[2] that exhibits a quasi-elliptical shape. The minor axis of the limit cycle ellipse increases and then decreases with increasing u_0, whereas the major axis monotonically decreases with increasing u_0. The slope of the major axis of the limit cycle,

$$\eta = (dq_i/dz)_{\text{maj}}, \tag{16}$$

decreases from β_i to 0 as u_0 increases from 0 to ∞.

The center of the limit cycle is located at the axis of rotation, $z = z_0 + \Delta Z/2$, and it is asymmetrically biased to the left side of $q_{\text{ad }i}(z)$ because of the nonlinear dependence of $q_{\text{ad }i}$ on z. For fluctuations with $\Delta Z < 700$ m, we can assume $\beta_i(z) \approx$ const, and therefore the center of the limit cycle can be approximated by the intersection of $z = z_0 + \Delta Z/2$ and $q_{\text{ad }i}(z)$ to a high degree of accuracy. Following the assumption that $\beta_i(z) \approx$ const, the average size of ice particles for the limit cycle can be estimated with

$$\bar{r}_{\text{im}} = \left(\frac{3\rho_a q_{\text{im}}}{4\pi\rho_i N_i}\right)^{1/3}, \tag{17}$$

where q_{im} is the adiabatic ice water mixing ratio at the center of limit cycle, which in turn can be estimated from Eq. (9) as

$$q_{\text{im}} = (q_{i0} + \delta q_i) + \beta_i \frac{\Delta Z}{2}. \tag{18}$$

Analogous to q_{im} the average temperature (T_m) for the limit cycle can be estimated as the ice adiabatic temperature at the center of rotation; that is,

$$T_m = T_0 + \delta T_i + \gamma_i \frac{\Delta Z}{2}. \tag{19}$$

For the limit cycles shown in Fig. 8, the centers of rotation (indicated by stars) are located at the same point in Q–Z coordinates, since initial conditions and ΔZ for all four cases are the same. It follows that the average sizes of the ice particles are also the same for

[2] A *limit cycle* is a closed trajectory to which the solution of a differential equation asymptotically approaches when $t \to +\infty$. In this work we consider *stable* limit cycles only.

all four cases. Substituting N_i, r_{i0}, S_{i0} and solving Eqs. (16)–(18) and (11) yields $\bar{r}_{\text{im}} = 32\mu\text{m}$ and $\tau_{\text{ph}} \approx 220\text{s}$.

The characteristic time of the vertical fluctuations can be estimated as $\tau_z = \Delta Z/\bar{u}_z$, where $\bar{u}_z = (2u_0/\pi)$ is the root-mean-square velocity for the harmonic oscillations and for the cases shown in Figs. 8a,b,c,d the characteristic time of the vertical fluctuations is $\tau_z \approx 1.6 \times 10^4$ s, 1.6×10^3 s, 310 s, and 62 s, respectively.

As can be seen in Fig. 8, the behavior of $q_i(z)$ during harmonic fluctuations is in agreement with the previous discussion. If $\tau_z \gg \tau_{\text{ph}}$, then $q_i(z)$ is close to the adiabatic ice water mixing ratio $q_{\text{ad}\,i}(z)$ (Fig. 8a). If $\tau_z \ll \tau_{\text{ph}}$, then the fluctuations take place as if they were made in cloud-free air (cf. Fig. 2, line AD) and the values of q_i and r_i during such fluctuations remain approximately constant (Fig. 8d). The cases shown in Figs. 8b,c are intermediate cases between $\tau_z \gg \tau_{\text{ph}}$ and $\tau_z \ll \tau_{\text{ph}}$.

b. *Activation of liquid phase during vertical harmonic oscillations*

Figure 9 shows a conceptual diagram of the activation of liquid water in ice clouds for two limit cycles of $q_i(z)$ formed during harmonic oscillations that have relatively large tangential velocities such that $\eta \approx 0$ [see Eq. (16)]. The limit cycle (1) has the center of rotation at point O_1 and the amplitude of the vertical oscillations is $\Delta Z = 2\Delta Z_c$. When the parcel reaches point A_1 the vapor pressure reaches water saturation. However, the activation of liquid water does not occur because the vertical component of the velocity $u_z = u_0 \sin(\pi) = 0$ at A_1 and it is below the threshold velocity. The limit cycle (2) rotates around point O_2, and its vertical amplitude is $\Delta Z > 2\Delta Z_c$. The activation of liquid water occurs at point A_2, and the layer $\Delta h \approx A_2B_2$ is mixed-phase layer with a thickness of

$$\Delta h = \frac{\Delta Z}{2} - \Delta Z_c. \tag{20}$$

From Fig. 9 it can be seen that activation and evaporation of liquid water during harmonic oscillations occurs at different altitudes. Therefore, it is clear that Eq. (20) gives an average value of the mixed-phase layer formed during the oscillations even when $\eta \approx 0$. For cases where $\eta > 0$, Eq. (20) does not necessarily represent the thickness of the mixed-phase layer, as we shall see later. However, in order to estimate what the minimum tangential velocity required for an oscillating ice cloud parcel to activate liquid water is, we will continue with the assumption that $\eta \approx 0$.

For the formation of a mixed-phase layer with $\Delta h > 0$ during harmonic oscillations, Eq. (20) yields the condition

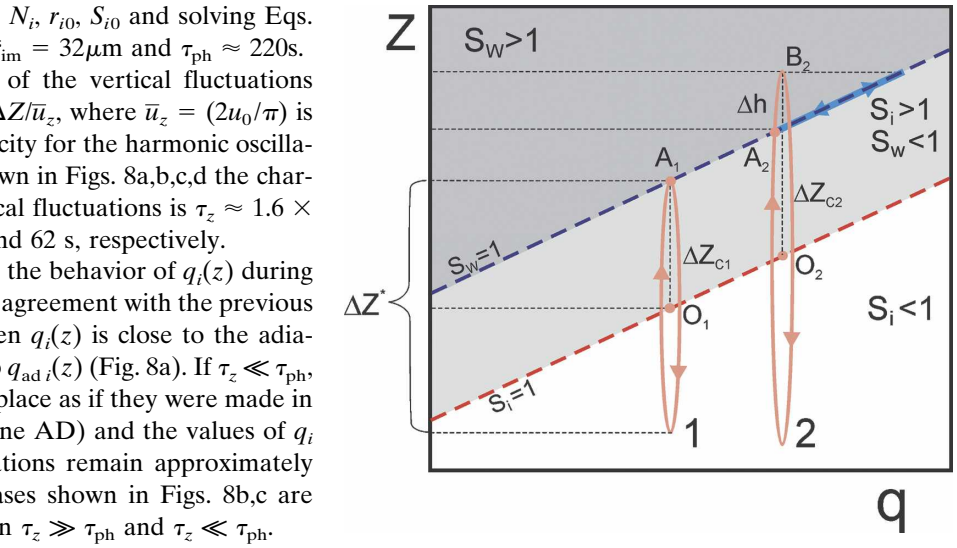

FIG. 9. Conceptual diagram of the activation of liquid water during vertical fluctuations.

$$\Delta Z > 2\Delta Z_c. \tag{21}$$

The vertical velocity at point A_2 can be calculated as

$$u_z = u_0 \sqrt{1 - 4\frac{\Delta Z_c^2}{\Delta Z^2}}. \tag{22}$$

By further assuming that at the point A_2 the vertical velocity u_z is equal to the threshold velocity, rearranging Eq. (22) and substituting u_z^* and u_0^* for u_z and u_0, respectively, yields the tangential velocity necessary for reaching saturation over water when the limit cycle is reached during harmonic oscillations:

$$u_0^* = \frac{u_z^* \Delta Z}{\sqrt{\Delta Z^2 - 4\Delta Z_c^2}}. \tag{23}$$

After modifying and substituting u_z^* [Eq. (1)], ΔZ_c [Eq. (5)], and introducing an empirical factor, k_0, Eq. (23) can be transformed into

$$u_0^* = \frac{k_0 b_m B_0 (E_w - E_i) N_i \bar{r}_{\text{im}} \Delta Z}{a_w E_i \sqrt{\Delta Z^2 - \dfrac{4}{a_w^2} \ln^2\left(\dfrac{E_w}{E_i}\right)}}. \tag{24}$$

The values of $\bar{r}_{\text{im}}$, q_{im}, and T_{im} required for calculation of Eq. (24) can be estimated using those appropriate for the center of rotation of the limit cycle from Eqs. (17)–(19), respectively. Eq. (24) contains an empirical factor k_0 that provides good agreement between the predicted threshold tangential velocity and the modeled value (see below).

Derived from the conditions stated in section 2, Eqs. (21) and (24) give the necessary and sufficient condi-

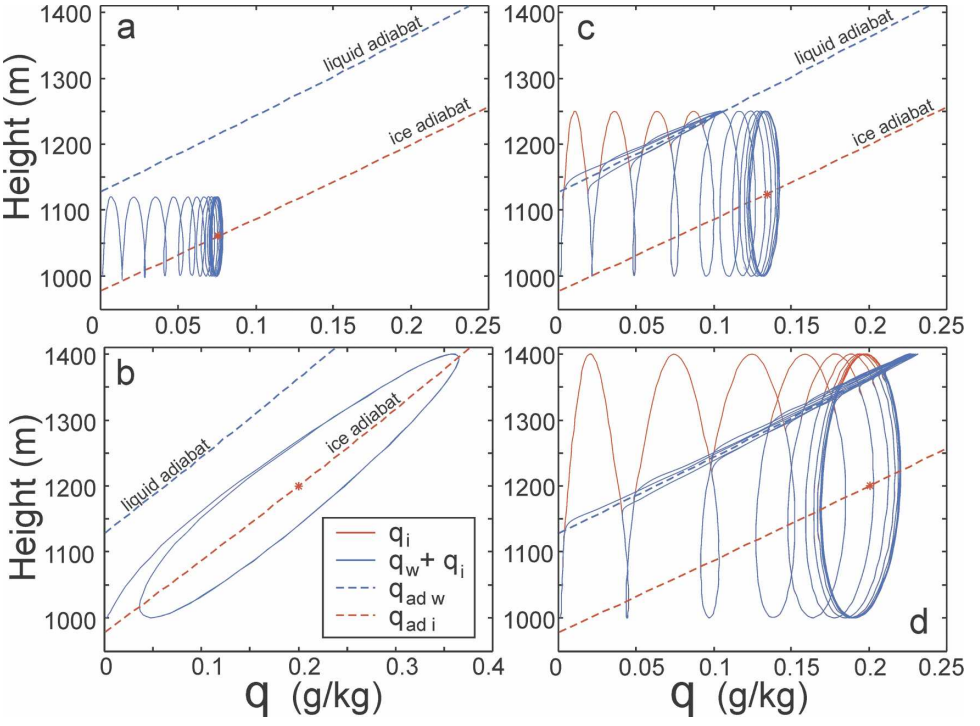

FIG. 10. Numerical modeling of the activation of liquid water in ice cloud during vertical harmonic oscillations. For all four cases $N_i = 50\ \mathrm{L}^{-1}$, $r_{i0} = 20\ \mu\mathrm{m}$, $S_{i0} = 0.01$, $T_0 = -10°\mathrm{C}$, and $\Delta Z_C = 153$ m. (a) Here $\Delta Z = 125$ m, $u_0 = 0.5\ \mathrm{m\ s^{-1}}$, and $u_z^* = 0.08\ \mathrm{m\ s^{-1}}$; (b) $\Delta Z = 400$ m, $u_0 = 0.05\ \mathrm{m\ s^{-1}}$, and $u_z^* = 0.12\ \mathrm{m\ s^{-1}}$; (c) $\Delta Z = 250$ m, $u_0 = 1\ \mathrm{m\ s^{-1}}$, and $u_z^* = 0.10\ \mathrm{m\ s^{-1}}$; and (d) $\Delta Z = 400$ m, $u_0 = 1\ \mathrm{m\ s^{-1}}$, and $u_z^* = 0.12\ \mathrm{m\ s^{-1}}$. The red star indicates the expected center of the limit cycle for an ice-only case.

tions for the formation of mixed phase during vertical harmonic oscillations of an ice cloud parcel. It should be noted that the physically meaningful existence of u_0^* in Eq. (24) [and u_0 in Eq. (22)] depends upon condition Eq. (21) being satisfied. In analogy to the conditions given in section 2 we can write the conditions appropriate for the harmonic oscillation:

Necessary and sufficient conditions for the activation of liquid water (at the limit cycle) within a parcel of ice cloud undergoing harmonic oscillations: (1) the amplitude must exceed a threshold amplitude [Eq. (21), and (2),] the tangential velocity of the oscillation must exceed a threshold velocity [Eq. (24)].

Figure 10 shows some numerical modeling results of the activation of liquid water within an ice cloud parcel during harmonic oscillations, and it illustrates how satisfying the first and/or second necessary conditions may or may not result in the activation of liquid water within ice clouds. Figure 10a shows the case when the tangential velocity condition is satisfied, but the vertical displacement is insufficient: $u_0 > u_0^*$, and $\Delta Z < 2\Delta Z_c$. For this case the activation of liquid water is not possible for any u_0. For the case shown in Fig. 10b, $\Delta Z > 2\Delta Z_c$, with $u_0 < u_0^*$, there is again no activation of liquid water, because this time the tangential velocity condition is not satisfied. For the case shown in Fig. 10c, where $u_0 > u_0^*$ and $\Delta Z_c < \Delta Z < 2\Delta Z_c$, activation of water occurs only during the first few cycles, but as $q_i(z)$ approaches the limit cycle $\Delta Z < 2\Delta Z_c$, and the activation of water is discontinued. In Fig. 10d both conditions $u_0 > u_0^*$ and $\Delta Z > 2\Delta Z_c$ are satisfied, and the activation and evaporation of liquid water occurs repeatedly.

In the discussion above we were concerned with the case when $\eta \approx 0$. Figure 11 shows that the evolution of parcels undergoing harmonic oscillations when $\eta > 0$ can exhibit behavior extremely different from that depicted in Fig. 9. It is clear from Fig. 11 that the parcels that are at the threshold tangential velocity u_0^* (Fig. 11a) or just exceed it (Fig. 11b) will activate water at lower altitudes than the maximum altitude of the oscillation and that the location of the mixed layer (A_1B_1 in Fig. 11b) also lies below an ice layer at the top of the oscillation. Increasing u_0 eventually results in the evaporation of liquid water during the descending branch of the limit cycle (A_2B_2 in Fig. 11c). With further increases in u_0, the altitude, at which activation and evaporation of liquid water occur, approaches a com-

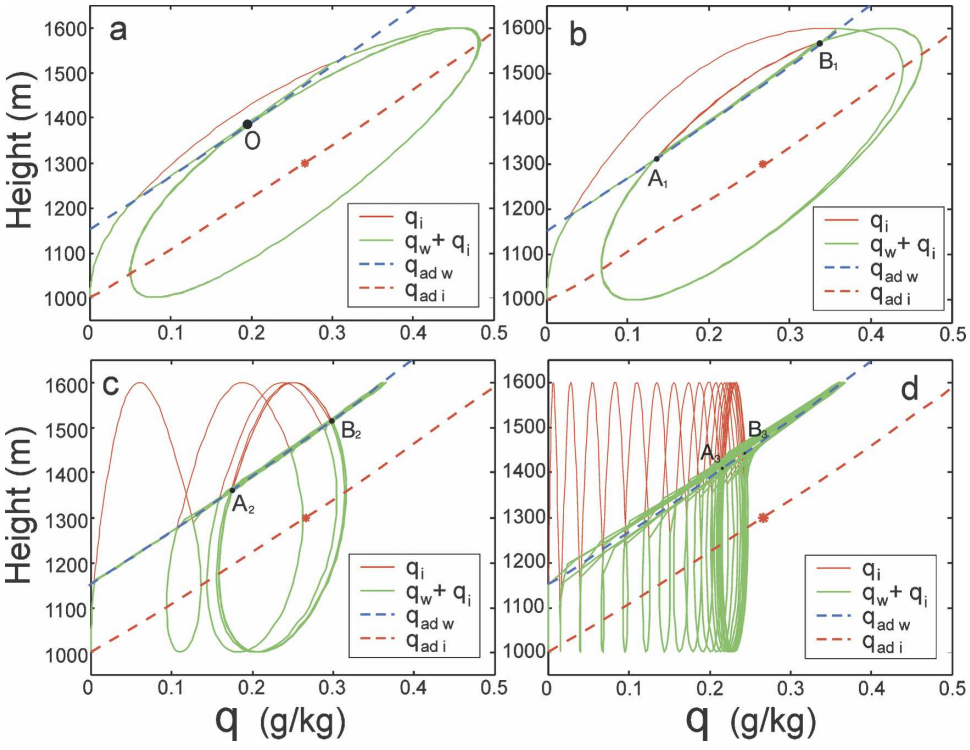

FIG. 11. Effect of vertical velocity on the formation of mixed phase during harmonic oscillations. (a) Here $u_0 = 0.22$ m s^{-1}, saturation over water is reached at a single point O, no activation of liquid water occurs once the limit cycle is reached; (b) $u_0 = 0.3$ m s^{-1}, after reaching a limit cycle both activation (point A_1) and evaporation (point B_1) of liquid water occurs during ascent; (c) $u_0 = 1$ m s^{-1}, activation of liquid water (point A_2) occurs during ascent and whereas evaporation (point B_2) during descent; and (d) $u_0 = 5$ m s^{-1}, activation (point A_3) and evaporation (point B_3) of liquid water occurs at approximately the same level. Numerical simulation was conducted for $T_0 = -10°$C, $r_{i0} = 10$ μm, $N_i = 100$ L^{-1}, $c = 0.5$, and $S_i = 0.01$. The red star indicates the expected center of the limit cycle for an ice-only case.

mon value (A_3B_3 in Fig. 11d). It can also be seen (Figs. 11c,d) that when water is activated, the center of the limit cycle is offset to the left of the location suggested by the ice-only analysis. This offset to lower condensed water values compensates for the excursions to higher condensed water mixing ratios along the liquid adiabat allowed by the activation of water compared to the ice-only case (cf. Fig. 8d and Fig. 11d).

Analogous to the approach in Fig. 6b, we have constructed a *U–Z* diagram (Fig. 12). Trajectories for different parcels occupy vertical lines with the relevant tangential velocity of the harmonic oscillation shown in Fig. 11. Thus, the case depicted in Fig. 11a is represented in Fig. 12 by a vertical line that just intercepts the point O. The case in Fig. 11b activates liquid at a lower altitude than point O as it crosses line 1 in point A_1. Then, as the vertical velocity falls below u_z^*, the liquid water eventually evaporates by the time the parcel crosses line 2 at point B_1 and returns to the ice phase only as it continues its ascent. The case in Fig. 11c is closer to that depicted in Fig. 9 and shows that the liquid is activated and maintained to the top of the oscillation (line 3). Subsequently the parcel remains mixed phase during the descent (region "b") until the liquid eventually evaporates as the parcel recrosses line 2. As seen from Fig. 12 for $u_z \to \infty$ lines 1 and 2 asymptote toward the same altitude.

Figure 13 shows a comparison of the threshold tangential velocity calculated from Eq. (24) with that obtained from numerical simulations of the activation of liquid water within ice clouds. The modeling was conducted for different amplitudes of harmonic oscillations (340 m $< \Delta Z <$ 800 m) and velocities (0.05 m s^{-1} $< u_0 <$ 6 m s^{-1}). The concentration of ice particles in different runs varied from 50 to 5000 L^{-1}. The empirical coefficient for this case was found to be $k_0 = 0.8$. The good agreement depicted in Fig. 13 supports the theoretical framework developed in the present study for adapting the necessary conditions described in section 2 to the special case of harmonic oscillations.

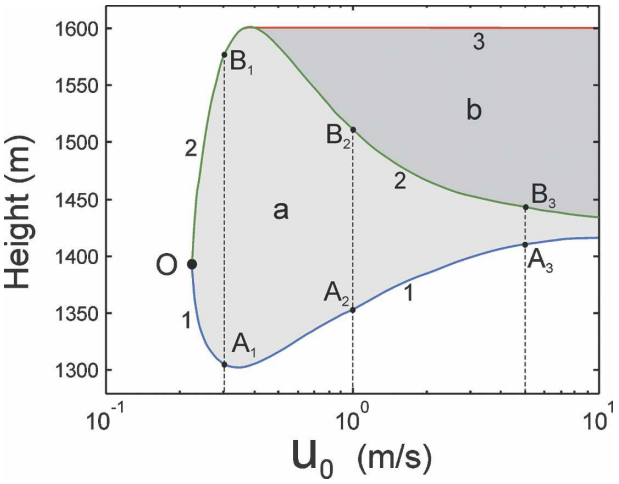

FIG. 12. Regions of mixed-phase zones in U–Z (tangential velocity–height) coordinates calculated for harmonic oscillations with $\Delta Z = 600$ m, $T_0 = -10°$C, $r_{i0} = 10$ μm, $N_i = 100$ L^{-1}, and $c = 0.5$ (as in Fig. 11). Line 1 indicates the altitude of activation of liquid water. Line 2 indicates altitude of liquid water evaporation. Line 3 is the maximum altitude of the oscillations. Shaded areas show (a) a region where mixed phase is formed during ascent (light shade), and (b) mixed phase exists during both ascent and descent. Point O corresponds to point O in Fig. 11a (dark shade). Points (A_1, B_1), (A_2, B_2), and (A_3, B_3) correspond to the points in Figs. 11b, 11c, and 11d, respectively.

5. Turbulent fluctuations

In the two previous sections we considered the evolution of mixed-phase conditions under regular vertical motions, for example, uniform ascents and harmonic oscillations. However, regular vertical motions in the atmosphere are limited in time and space. Typically vertical motions in clouds have a turbulent nature. We have attempted to carry out an initial exploration of the effects of turbulent motion on the evolution of mixed-phase cloud by randomly sampling updraft velocities from a normal distribution with a standard deviation of σ_u and zero mean, at each time step, Δt. The vertical motion was limited by upper and lower boundaries; that is, $Z_1 < z < Z_2$. The upper and lower boundaries were considered to be perfectly elastic: if a modeled parcel intersected the upper or lower boundaries, the current velocity of the parcel motion was reversed for the remainder of the time step.

The choice of Δt is important for the integration and we have made it consistent with the imposed scale and vertical velocity variance. The Lagrangian decorrelation time scale is given as (Rodean 1996)

$$\tau_d = \frac{2\sigma_u^2}{\varepsilon C_0}, \tag{25}$$

where ε is the turbulent kinetic energy dissipation rate and C_0 is the Lagrangian structure function ($C_0 \sim 4$, Rodean 1996). If we assume that the turbulent kinetic energy is equal to the integrated Kolmogorov energy spectrum for the inertial subrange only for scales *smaller* than ΔZ we find that

$$\sigma_u = 0.7\varepsilon^{1/3}\Delta Z^{1/3}, \tag{26}$$

and hence, substituting Eq. (26) into Eq. (25) yields the decorrelation time scale

$$\tau_d = \frac{0.17\Delta Z}{\sigma_u}. \tag{27}$$

It should be noted that the decorrelation time has its own probability distribution function, and Eq. (27) gives an estimate of a characteristic value of τ_d.

The purpose of this model is to simulate irregular vertical motions in a stratiform layer limited by $Z_1 = 800$ m and $Z_2 = 1500$ m. For a vertical velocity $u_z(t)$ with $\sigma_u = 0.75$ m s^{-1} the time step was calculated as $\Delta t = \Delta t_c + \Delta t_r$, where $\Delta t_c \sim \tau_d$ was assumed to be constant and it was calculated from Eq. (27) ($\Delta t_c = 160$ s) and the random component Δt_r varied in the range $-60 < \Delta t_r < 60$ s. Examination of the distribution of velocities u_z (not shown) reveals that it is close to normal with $\sigma_u = 0.75$ m s^{-1} and that the distribution of parcel altitudes was approximately uniform.

Trajectories of $q_i(z)$ and $q_i(z) + q_w(z)$ modeled for the vertical motion $u_z(t)$ are presented in Fig. 14a. Figure 14b shows mean values of $q_i(z)$ and $q_w(z)$ averaged over the whole integration period. Dashed lines in Fig. 14b indicate the maximum to minimum envelope of modeled values as a function of height. Figure 14b shows that the average liquid water mixing ratio increases toward cloud top faster than the ice water mixing ratio—a behavior that is often observed in stratiform mixed-phase clouds for liquid water content, but not generally for ice water content. Instead, ice water content is usually observed to be fairly constant with height, or shows increased values near the base of the cloud (e.g., Pinto 1998; Fleishauer et al. 2002). We also considered the influence of the decorrelation time on the results obtained using random fluctuations. If the decorrelation time was too short, liquid would never activate; if the decorrelation time was too long, the elastic boundary conditions of our model would lead to a sawtooth motion for the parcel producing results similar to those obtained for the harmonic oscillations.

We have also modeled a harmonic oscillation with the same initial conditions and the same vertical velocity variance as the turbulent realization for comparison.

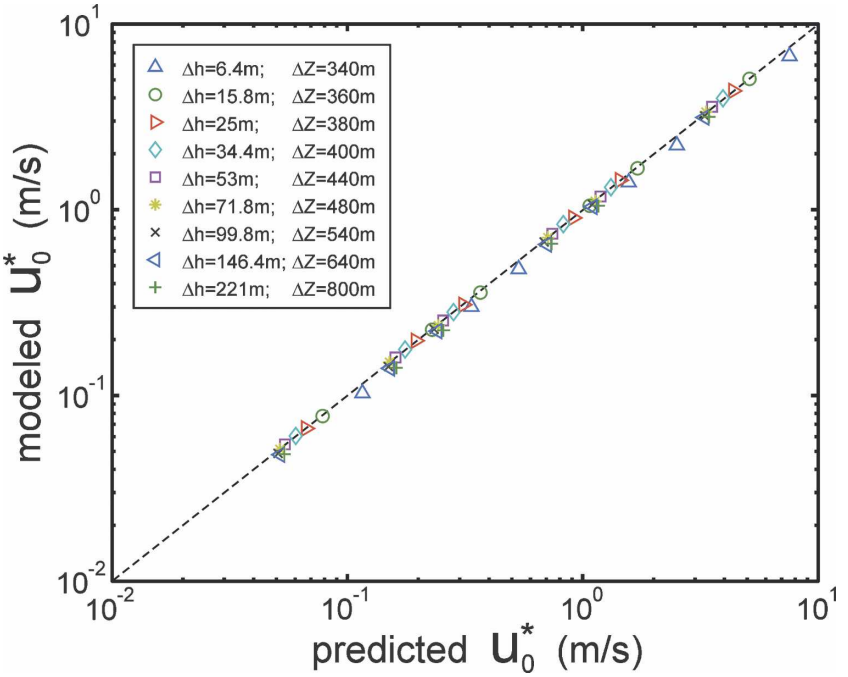

FIG. 13. Comparison of the theoretical threshold velocity u_0^* [Eq. (24)] and that deduced from numerical modeling of activation of liquid water in liquid clouds. Here $T_0 = -10°C$, 340 m $< \Delta Z <$ 800 m, 0.05 m s$^{-1} < u_0 <$ 6 m s^{-1}, 50 L$^{-1} < N_i <$ 5000 L^{-1}, $H_0 = 1000$ m, $c = 0.5$, and $k_0 = 0.8$.

The results of this modeling are shown in Fig. 15. As seen from comparisons of Fig. 15b and Fig. 14b, the harmonic oscillation on average produces more liquid water and a lower ice water mixing ratio than the turbulent realization.

One of the main conclusions that we can draw from these modeling experiments is that turbulent vertical fluctuations alone prevent formation of limit cycles. Wave structures are often observed in clouds and it is likely that real motions consist of some combination of

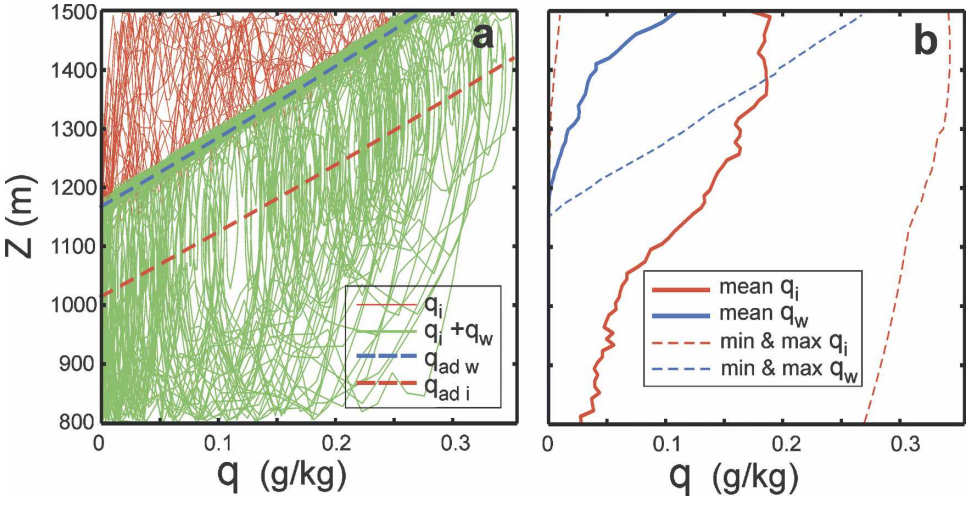

FIG. 14. Numerical simulation of formation of mixed phase during turbulent fluctuations. (a) Trajectories of ice $q_i(z)$ (red line) and total $q_i(z) + [q_w(z)]$ (green line) water mixing ratios. Dashed lines are adiabatic ice and liquid mixing ratios. (b) Averaged ice $[q_i(z)]$ (thick red) and liquid $[q_w(z)]$ (thick blue) water mixing ratios. Dashed lines indicate maximum and minimum values. Modeling has been performed for the vertical fluctuations with $\sigma_u = 0.75$ m s^{-1}, $r_{i0} = 20$ μm, $N_i = 50$ L^{-1}, and $T_0 = -10°C$.

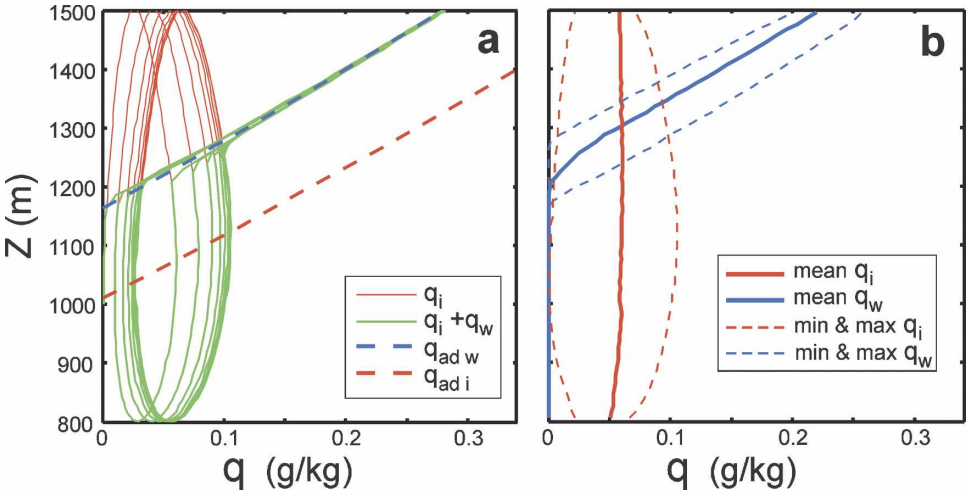

FIG. 15. Modeling of the formation of mixed phase during harmonic oscillations with the same σ_u, r_{i0}, N_i, and T_0 as for the case of turbulent fluctuations shown in Fig. 14.

wave and turbulent fluctuations. The profiles of liquid and ice water mixing ratio obtained during both turbulent and harmonic oscillations are similar to those observed in stratiform mixed-phase clouds.

6. Discussion

Before we look at the implications of these results to the real atmosphere we should consider the possible impacts of the simplifying assumptions that were used in the model. In general, changes to any of the assumptions will cause changes to the vapor source/sink terms for ice and liquid. Decreases (increases) in the vapor uptake to the ice phase will result in a decrease (increase) to the threshold velocity [Eq. (1)] required to generate a mixed-phase cloud.

There are two main issues to consider: i) the representation of the particles in the parcel, and ii) sedimentation. For droplets, introducing more complex assumptions will have little impact on the vapor source/sink ability of the liquid phase. Test computations including the growth of haze and activation of droplets indicated only minor changes in the outcome of the modeling. If parcel uplift time scales exceed the sedimentation time scales, the sink/source of vapor to the liquid phase will be overestimated.

For ice crystals the assumptions made in the model lead to a number of possible problems. The choice of shape controls the particle size for a given concentration and ice water content. Additionally, the shape dictates the capacitance of the ice crystals that controls the diffusional growth rate, which is also modified by the ventilation coefficient. To some extent using the capacitance of a sphere for ice crystals is offset by ignoring ventilation effects. The spherical assumption leads to the prediction of smaller mean crystal sizes than is typically observed, and the lack of aggregation and sedimentation means that vapor source/sink rates to the ice phase will be overestimated for isolated thin mixed-phase clouds by the model. In fact, continued sedimentation will result in the removal of all ice nuclei and the mixed-phase layer will be converted to a stable supercooled liquid layer. If the mixed layer is embedded within a deep ice cloud then the effects of sedimentation will not be as drastic: particles falling out of the mixed-phase layer will be replaced by similar particles falling in from above. Riming converts liquid droplets directly to ice and should be represented in appendix E as another rate equation proportional to q_w and the second moment of the ice particle size distribution. However, ignoring this process could be viewed approximately as effectively underestimating the sink of water vapor to the ice phase.

Figure 16 schematically summarizes the variety of situations covered in this paper in which liquid water was activated within an ice cloud to generate mixed phase. Given sufficiently high initial velocities, the uniform vertical ascents will eventually activate and generate a layer of mixed phase, but will eventually lose all activated liquid as the sink to the ice phase grows with altitude or due to homogeneous freezing after reaching temperatures colder than −40°C (Fig. 16a). Such cases may be applicable to embedded convection within frontal cloud associated with midlatitude cyclones, or possibly to stable upslope cloud conditions. If clouds have internal motions that are well described as harmonic

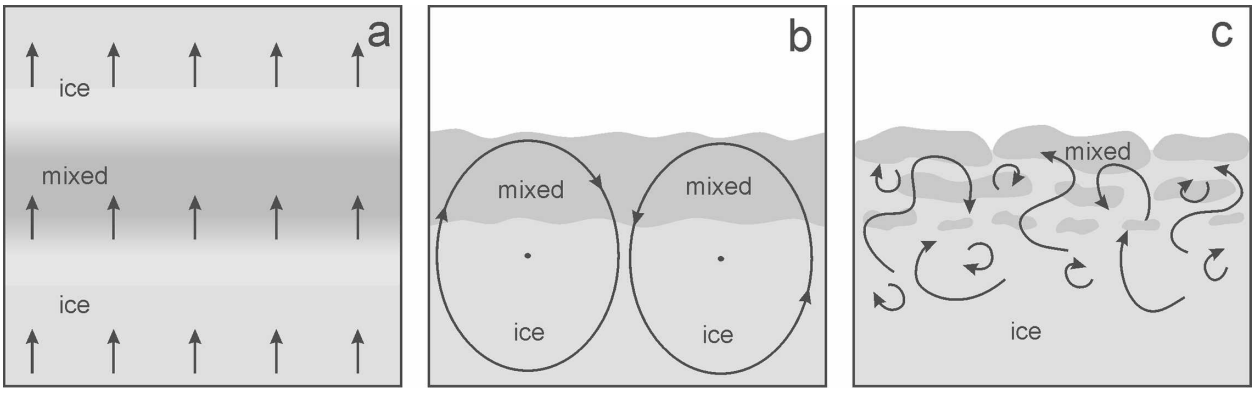

FIG. 16. Conceptual diagrams of the three mixed-phase scenarios considered: (a) uniform ascent, (b) harmonic oscillations, and (c) turbulent fluctuations.

with sufficient amplitude and tangential velocity, they will exhibit a relatively uniform mixed-phase layer (Fig. 16b). If the internal motion of the cloud is more turbulent in nature then any mixed-phase layer will be more inhomogeneous when compared to the harmonic case (Fig. 16c).

The original motivation for studying the activation of liquid water during harmonic oscillations came from the idea that the evolution of parcels subjected to this motion would represent midlevel-layer cloud and provide an explanation for the often observed liquid layers that exist at the top of layer cloud. It is perhaps not too surprising given the constraints used in the turbulent case that we find a similar picture to that of the oscillations with a long-lived, but more intermittent layer of liquid water at the top of an ice cloud layer. As well as supercooled-layer clouds, the turbulent and oscillatory scenarios may also be applicable to deeper stratiform ice cloud where shear layers within the cloud can generate gravity waves and turbulence. Such mixed-phase cloud layers are not uncommon and they can be observed inside deep frontal glaciated nimbostratus. In many cases the dynamically forced boundary layer stratocumulus may be formed in ice precipitation generated by upper-clouds.

Prognostic water schemes can be found in many numerical weather prediction models (e.g., Wilson and Ballard 1999) and so those schemes could potentially reproduce the results presented here. The difficulty large-scale models face relates to the coarse grid spacings that are currently required for practical applications. To overcome this we suggest the following approach. Since we have seen that bounded turbulence produces mean results similar to that seen for harmonic oscillations with the same velocity variance, it is tempting to suggest that we could attempt to diagnose the subgrid vertical velocities via a turbulence closure scheme and then assign all of the diagnosed turbulent kinetic energy to a single mode of oscillation at the scale of the grid box. Consequently, grid box water mixing ratios can then be repartitioned appropriately if additional supercooled liquid water is diagnosed.

The necessary and sufficient conditions given in section 2 are only applicable when considering the activation of liquid water within ice cloud. Once liquid has been produced it provides a reservoir that can maintain the cloud in mixed phase even when the vertical velocity falls below the threshold velocity [Eq. (1)]. This is seen very clearly in some of the harmonic oscillation results (e.g., Fig. 11) where the vertical velocity can fall to zero and even go negative while the cloud remains in mixed phase.

Previous studies that have derived threshold updraft velocities required for maintaining steady-state mixed-phase conditions are essentially considering a single altitude in Fig. 16a within the mixed-phase region. We believe that by considering the nonequilibrium evolution of an idealized mixed-phase parcel we have been able to explore some of the richness of the three-phase ice–liquid–vapor system. By not making the initial assumption of steady state we have demonstrated that nonequilibrium evolution can lead to the long-term steady existence of mixed-phase conditions.

7. Conclusions

We have identified and demonstrated using a parcel model the conditions required to activate liquid water within an ice cloud:

Necessary and sufficient conditions for the activation of liquid water within an ice cloud parcel require (1) the vertical velocity to exceed a threshold velocity, and (2) a vertical ascent above some threshold altitude.

Similarly we were able to identify subsidiary conditions concerning tangential velocity and amplitude for the special case of harmonic oscillations.

After sufficient time for the harmonic oscillations a limit cycle was reached, in which the microphysical parameters such as particle size, condensed water, supersaturation and temperature oscillated around a constant mean. If the limit cycle was able to activate liquid water during a part of the revolution, then a mixed-phase cloud would be produced repeatedly.

Turbulent vertical velocity fluctuations do not produce limit cycles, but may also lead to the production of long-lived mixed-phase cloud. The amount of liquid water activated during turbulent fluctuations decreases with a decrease in the decorrelation time of the fluctuations, and on average it is always less than harmonic oscillations carried out over the same vertical extent with the same σ_u.

Acknowledgments. Authors express gratitude to and three anonymous reviewers and Ilia Mazin for their useful comments.

APPENDIX A

List of Symbols

Symbol	Description	Units
a_w	$\frac{g}{R_a T}\left(\frac{L_w R_a}{c_p R_v T} - 1\right)$	m^{-1}
a_i	$\frac{g}{R_a T}\left(\frac{L_i R_a}{c_p R_v T} - 1\right)$	m^{-1}
A	$-b_i B_i N_i \bar{r}_i$	s^{-1}
A_i	$\left(\frac{\rho_i L_i^2}{k R_v T^2} + \frac{\rho_i R_v T}{E_i(T) D}\right)^{-1}$	$m^2\,s^{-1}$
A_w	$\left(\frac{\rho_w L_w^2}{k R_v T^2} + \frac{\rho_w R_v T}{E_w(T) D}\right)^{-1}$	$m^2\,s^{-1}$
b_i	$\frac{1}{q_v} + \frac{L_i^2}{c_p R_v T^2}$	—
b_m	$\frac{1}{q_v} + \frac{L_w L_i}{c_p R_v T^2}$	—
b_w	$\frac{1}{q_v} + \frac{L_w^2}{c_p R_v T^2}$	—
B	$\left(\frac{p R_v}{E_i R_a} + \frac{L_i^2}{c_p R_v T^2}\right) B_i N_i \bar{r}_i - a_i u_z$	s^{-1}
B_0	$\frac{4\pi c \rho_i A_i}{\rho_a}$	$m^2\,s^{-1}$
B_i	$b_i B_0$	$m^2\,s^{-1}$
B_i^*	$b_m B_0\left(\frac{E_w}{E_i} - 1\right)$	$m^2\,s^{-1}$
c	Ice particle shape factor characterizing "capacitance" $0 < c \leq 1$ ($c = 1$ for spheres)	—
c_p	Specific heat capacity of moist air at constant pressure	$J\,kg^{-1}K^{-1}$
C	$a_i u_z$	s^{-1}
C_0	Lagrangian structure function ($C_0 \sim 4$)	—
D	Coefficient of water vapor diffusion in the air	$m^2\,s^{-1}$
e	Water vapor pressure	$N\,m^{-2}$
E_i	Saturation vapor pressure above flat surface of ice	$N\,m^{-2}$
E_w	Saturation vapor pressure above flat surface of water	$N\,m^{-2}$
$f(r_i, \rho_i, c)$	Distribution of ice particle sizes, density, and capacitance normalized on unity	$m^2\,kg^{-1}$
g	Acceleration of gravity	$m\,s^{-2}$
k	Coefficient of air heat conductivity	$J\,m^{-1}s^{-1}K^{-1}$
k_0	Empirical coefficient	—

Symbol	Description	Units
L_i	Latent heat for ice	J kg^{-1}
L_w	Latent heat for liquid water	J kg^{-1}
N_i	Concentration of ice particles	m^{-3}
N_w	Concentration of liquid droplets	m^{-3}
p	Pressure of moist air	N m^{-2}
p_a	Pressure of dry air	N m^{-2}
$q_{\text{ad } i}$	Adiabatic ice water mixing ratio (mass of ice per 1 kg of dry air)	—
$q_{\text{ad } w}$	Adiabatic liquid water mixing ratio (mass of ice per 1 kg of dry air)	—
q_{im}	Average ice water mixing ratio of a limit cycle	—
q_i	Ice water mixing ratio (mass of ice per 1 kg of dry air)	—
q_v	Water vapor mixing ratio (mass of water vapor per 1 kg of dry air)	—
q_w	Liquid water mixing ratio (mass of liquid water per 1 kg of dry air)	—
r_i	Half of a maximum linear dimension of an ice particle	m
$\bar{r}_{\text{im}}$	Mean ice particle half-size averaged over a limit cycle	m
r_w	Liquid droplet radius	m
R_a	Specific gas constant of moist air	J kg^{-1}K^{-1}
R_v	Specific gas constant of water vapor	J kg^{-1}K^{-1}
S_{qs}	Quasi-steady supersaturation	—
S_i	e/E_i-1, supersaturation over ice	—
S_w	e/E_w-1, supersaturation over water	—
t	Time	s
T	Temperature	K
T_m	Average temperature of a limit cycle	K
u_z	Vertical velocity	m s^{-1}
$u^*_{z\,\min}$	Minimum vertical velocity which allows activation of liquid water in a uniformly ascending adiabatic ice cloud	m s^{-1}
u^*_z	Critical vertical velocity required for activation of liquid water in an ice cloud	m s^{-1}
u_0	Tangential velocity of a cloud parcel during harmonic oscillations	m s^{-1}
u^*_0	Tangential velocity of a cloud parcel required for formation of mixed phase in a layer Δh after reaching a limit cycle	m s^{-1}
z	Altitude	m
Z_c	Minimum altitude at which adiabatic parcel reaches saturation over liquid water	m
$Z^*_{\max}$	Maximum altitude at which uniformly ascending adiabatic ice cloud may reach saturation over water	m
β_i	$\left(\frac{dq_i}{dz}\right)_{\text{ad}} = \frac{a_i}{b_i}$ Vertical adiabatic gradient of ice mixing ratio	m^{-1}
β_w	$\left(\frac{dq_w}{dz}\right)_{\text{ad}} = \frac{a_w}{b_w}$ Vertical adiabatic gradient of water mixing ratio	m^{-1}
γ_{i}	Ice adiabatic lapse rate	K m^{-1}
δq_i	Isobarically condensed or sublimated ice water mass required to bring the air in a cloud parcel to saturation over ice	—
δT_i	Temperature change related to isobaric condensation or sublimation of ice (with the mixing ratio δq_i) required to bring the air to saturation over ice	K
Δh	Vertical depth of a cloud layer above the level of activation of liquid water	m
Δt	Time step during which the vertical velocity was kept constant in modeling of turbulent fluctuations	s
ΔZ	Amplitude of vertical harmonic oscillations	m
ΔZ_c	Vertical distance between ice and liquid water saturation levels [Eq. (5)]	m
ε	Turbulent kinetic energy dissipation rate	m^2 s^{-3}
η	$(dq_i/dz)_{\text{maj}}$ Slope of the major axis of a limit cycle of ice mixing ratio	m^{-1}
ζ	$A_i c \left(\frac{48\pi^2 \rho_i^2 N_i^2}{\rho_a^2}\right)^{1/3}$	s^{-1}
ρ_a	Density of the dry air	kg m^{-3}
ρ_i	Density of an ice particle	kg m^{-3}
ρ_w	Density of liquid water	kg m^{-3}
σ_u	Standard deviation of fluctuations of vertical velocity	m s^{-1}
τ_{ph}	Time of phase relaxation	s
τ_z	Characteristic time scale of vertical velocity fluctuations	s

Symbol	Description	Units
τ_d	Decorrelation time of turbulent vertical fluctuations	s
χ	$a_i\zeta$	$m^{-1}\ s^{-1}$
ϑ	$b_i\zeta$	s^{-1}

APPENDIX B

Change in Condensed Water Mixing Ratio for Ballistic ($u_z \to \infty$) and Adiabatic ($u_z \to 0$) Cases

Consider a Squires' equation (Squires 1952) for supersaturation in ice cloud:

$$\frac{1}{S_i + 1}\frac{dS_i}{dt} = a_i u_z - b_i B_i N_i \bar{r}_i S_i. \tag{B1}$$

Equation (B1) can be rewritten as

$$\frac{1}{S_i + 1}\frac{dS_i}{dz} = a_i - \frac{1}{u_z} b_i B_i N_i \bar{r}_i S_i. \tag{B2}$$

Since b_i, B_i, N_i, S_i, and $\bar{r}_i$ are finite values, the second term on the right side of Eq. (B2) will approach zero, as $u_z \to \infty$ (ballistic case). Hence, we obtain

$$\frac{1}{S_i + 1}\frac{dS_i}{dz} = a_i. \tag{B3}$$

Therefore, the relative humidity in clouds for $u_z \to \infty$ varies with altitude as if the ascent was carried out in cloud-free conditions. By comparing Eq. (B3) with the equation (see Korolev and Mazin 2003)

$$\frac{1}{S_i + 1}\frac{dS_i}{dz} = a_i - b_i \frac{dq_i}{dz}, \tag{B4}$$

it follows that $(dq_i/dz) \to 0$, if $u_z \to \infty$.

Assume that initially $q_{i0} > 0$ and $S_{i0} > 0$. Then, if the vertical velocity $u_z \to 0$, any excess vapor will be accommodated by existing ice particles, and eventually $(t \to \infty)$ supersaturation $S_i \to 0$. Under these circumstances $(dS_i/dz) \to 0$, and Eq. (B4) becomes

$$\frac{dq_i}{dz} = \beta_i, \tag{B5}$$

where $\beta_i = a_i/b_i$ is adiabatic vertical gradient of ice water mixing ratio; that is, condensed water will change along the adiabat, if $u_z \to 0$ (adiabatic case).

Thus, we arrive at the conclusion that, when the vertical velocity changes in the range $0 < u_z < \infty$, the gradient of condensed water changes in the range $\beta_i > (dq_i/dz) > 0$, respectively. Therefore, depending on u_z, the trajectory $q_i(z)$ may intersect the curve $q_{\mathrm{ad}\ w}(z)$, which has a gradient $(dq_{\mathrm{ad}\ w}/dz) = \beta_w \approx \beta_i$. Since $q_i[z(t)]$ is a continuous function, given sufficient vertical ascent, there is an ensemble of vertical velocities $u_z(t)$ resulting in trajectories $q_i(z)$ such that they intersect $q_{\mathrm{ad}\ w}(z)$.

Similar considerations regarding the behavior of condensed water at $u_z \to \infty$ and $u_z \to 0$ are equally applicable for liquid clouds.

APPENDIX C

Calculation of the Distance between Ice and Liquid Saturation Levels

Consider a simplified Squires equation for a liquid cloud (Squires 1952):

$$\frac{1}{S_w + 1}\frac{dS_w}{dt} = a_w u_z - b_w B_w N_w \bar{r}_w S_w. \tag{C1}$$

Here $S_w = (e/E_w) - 1$ is the supersaturation over water, e is the water vapor pressure, E_w is the saturated water vapor pressure over water, a_w is a coefficient dependent upon temperature, N_w and r_w are the concentration and radii of cloud droplets, and b_w and B_w are coefficients dependent upon pressure and temperature (see appendix A). In the absence of cloud particles the second term on the rhs will be equal to zero, and Eq. (C1) can be rewritten as

$$\frac{dS_w}{S_w + 1} = a_w dz. \tag{C2}$$

Integrating Eq. (C2) from the initial humidity $[S_{w0} = (e_0/E_w) - 1]$ to saturation over water $(S_w = 0)$ yields the distance between these two levels:

$$\Delta Z_c = \frac{1}{a_w} \ln\left(\frac{E_w}{e_0}\right). \tag{C3}$$

During integration of Eq. (C2) the coefficient a_w and saturated water vapor pressure E_w were assumed constant. The diagram in Fig. C1 justifies this approximation and shows a comparison of absolute and relative errors between ΔZ_c derived from Eq. (C3) and those calculated from numerical solution of the system of differential equations (appendix F) for three different initial relative humidities. As seen from Fig. C1b, the maximum relative errors for $e_0 = E_i$ do not exceed 2.2% and are sufficiently accurate for the present study.

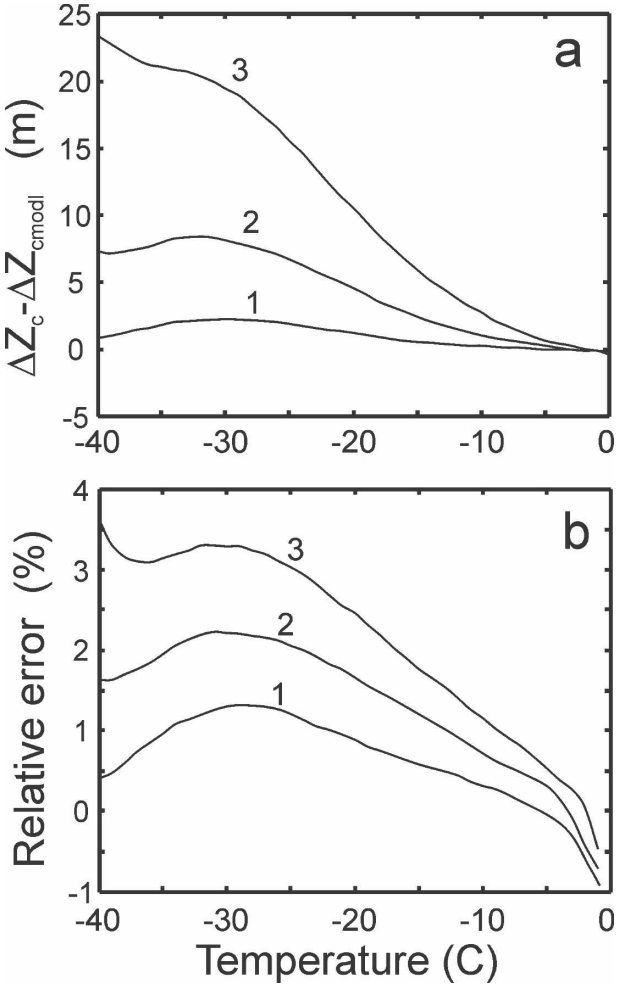

FIG. C1. (a) Absolute and (b) relative errors between ΔZ_c derived from Eq. (C3) and those calculated from numerical solution of the system of differential equations in appendix F. Initial humidity in the parcel: 1) $e_0 = E_i + (E_w - E_i/2)$ (supersaturation with respect to ice, midpoint between saturation over ice and liquid); 2) $e_0 = E_i$ (saturation with respect to ice); and 3) $e_0 = E_i - (E_w - E_i/2)$ (subsaturation with respect to ice).

APPENDIX D

Calculation of the Ice and Liquid Water Adiabat

Consider a cloud parcel with initial supersaturation $S_{i0} = [e_0/E_i(T_0)] - 1$, ice water mixing ratio q_{i0}, and temperature T_0 at level Z_0 (point A1 in Fig. D1). To find the ice adiabat associated with the point A1 the water vapor in the cloud parcel should be isobarically brought to saturation over ice ($S_{i1} = 0$), since the vapor pressure along the ice adiabat is saturated with respect to ice. During isobaric processes the air pressure stays constant and, therefore

$$p_{a0} + e_0 = p_{a1} + E_i(T_1). \tag{D1}$$

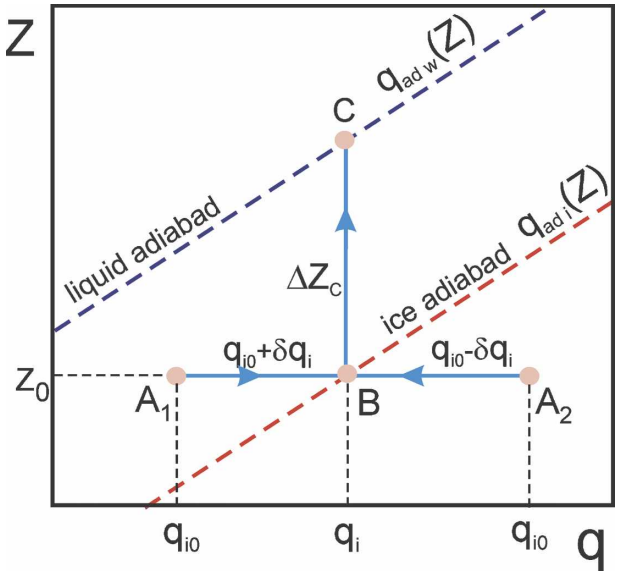

FIG. D1. Conceptual diagram explaining relationship between initial condition of a cloud parcel and associated liquid and ice adiabats.

Here p_{a0}, p_{a1} are the initial and final pressure of dry air, respectively; e_0 is initial water vapor pressure; and T_1 is a final temperature. After condensation from S_{i0} to S_{i1} the amount of condensed water will be $\delta q_i = q_{i0} - q_{i1}$, where q_{i0} and q_{i1} are initial and final water vapor mixing ratios, respectively. Therefore, the final mass of ice at point B will be $q_{i0} + \delta q_{i1}$. In other words the sum $(q_{i0} + \delta q_i)$ represents the adiabatic ice water mixing ratio at z_0. The values of q_{i0} and q_{i1} can be found as

$$q_{i0} = \frac{e_0}{p_{a0}} \frac{R_a}{R_v}, \tag{D2}$$

$$q_{i1} = \frac{E_i(T_1)}{p_{a1}} \frac{R_a}{R_v}. \tag{D3}$$

The temperature during isobaric condensation will change from T_0 to T_1, and can be found from the energy conservation equation

$$L_i \delta q_i = c_p \delta T; \tag{D4}$$

here $\delta T = T_0 - T_1$.

The values of δq_i and T_1 can be found through the numerical solution of Eqs. (D1)–(D4).

From point B the ice adiabat $q_{\mathrm{ad}\,i}$ can be calculated using

$$q_{\mathrm{ad}\,i}(z) = q_{i0} + \delta q_i + \int_{z_0}^{z} \beta_i(z')\, dz'. \tag{D5}$$

If the water vapor at the initial point is supersaturated (subsaturated), then this point will lie to the left

(right) of the adiabat in Q–Z coordinates (A1, A2, respectively). To find liquid adiabat, saturation over liquid water along the ballistic trajectory must first be reached. It can be accomplished by adiabatic ascent through a distance ΔZ_c from point B to C without condensation of ice (see appendix C). From point C the liquid adiabat can be calculated using

$$q_{\mathrm{ad}\,w}(z) = q_{i0} + \delta q_i + \int_{z_0+\Delta Z_c}^{z} \beta_w(z')\,dz'. \quad \text{(D6)}$$

In the above discussion it has been assumed that initial liquid water mixing ratio was $q_{w0} = 0$. If $q_{w0} \neq 0$, then it should be added to Eqs. (D5) and (D6).

APPENDIX E

Equation for Condensed Ice Mass in a Vertically Moving Adiabatic Parcel

Consider a Squires equation for an ice cloud adiabatic parcel in a form (e.g., Korolev and Mazin 2003):

$$\frac{1}{S_i + 1}\frac{dS_i}{dt} = a_i u_z - b_i \frac{dq_i}{dt}. \quad \text{(E1)}$$

The rate of changes in the ice water mixing ratio due to deposition growth or sublimation of ice particles can be described as

$$\frac{dq_i}{dt} = \frac{4\pi N_i}{\rho_a}\int_0^1 \int_{\rho_{i\,\min}}^{\rho_{i\,\max}} \int_0^\infty f(r_i, \rho_i, c)\rho_i r_i^2 \frac{dr_i}{dt}\,dr_i\,d\rho_i\,dc. \quad \text{(E2)}$$

Here N_i is the number concentration of ice particles; r_i is the characteristic size of ice particles; c is a shape factor of ice particles characterizing "capacitance" in the equation of the growth rate; ρ_i is the density of ice particles ($\rho_{i\min} < \rho_i < \rho_{i\max}$); and $f_i(r_i, \rho_i, c)$ is the distribution of ice particles by characteristic size, density, and shape factor normalized to unity. In the following, the size r_i is defined as half of the maximum dimension of the ice particle. The ice particle size r_i is related to the shape factor c through the rate of the mass growth. For the definition of r_i, accepted here, the shape factor varies in the range $0 < c \leq 1$, being equal to 1 for ice spheres.

The diffusional growth rate of the ice particles can be written as (e.g., Pruppacher and Klett 1997)

$$\frac{dr_i}{dt} = \frac{cA_iS_i}{r_i}. \quad \text{(E3)}$$

Then, substituting Eq. (E3) into Eq. (E2) and averaging over r_i and c gives

$$\frac{dq_i}{dt} = S_i \frac{4\pi\rho_i A_i N_i \overline{r_i c}}{\rho_a}. \quad \text{(E4)}$$

For simplicity we assume that c in Eq. (E4) is the same for all ice particles. Assuming ice particles are ice spheres and substituting the size-to-mass relationship $r_i = (3\rho_a q_i/4\pi\rho_i N_i)^{1/3}$ into Eq. (E4), gives

$$q_i^{-1/3}\frac{dq_i}{dt} = \zeta S_i, \quad \text{(E5)}$$

where $\zeta = A_i c(48\pi^2\rho_i^2 N_i^2/\rho_a^2)^{1/3}$. Then differentiating Eq. (E5) gives

$$q_i^{-1/3}\frac{d^2q_i}{dt^2} - \frac{1}{3}q_i^{-4/3}\left(\frac{dq_i}{dt}\right)^2 = \zeta\frac{dS_i}{dt}. \quad \text{(E6)}$$

Substituting S_i and dS_i/dt from Eqs. (E5) and (E6), respectively, into Eq. (E1) yields

$$\frac{d^2q_i}{dt^2} - \left(\frac{1}{3q_i} + b_i\right)\left(\frac{dq_i}{dt}\right)^2 + (\vartheta q_i^{1/3} - a_i u_z)\frac{dq_i}{dt} - \chi u_z q_i^{1/3} = 0; \quad \text{(E7)}$$

here $\vartheta = b_i\zeta$ and $\chi = a_i\zeta$.

An equation for liquid clouds can be obtained from Eq. (E7) by formal replacing subscripts "i" by "w" in q and coefficients a_i, b_i, χ, and ϑ, and assuming $c = 1$ for droplets.

APPENDIX F

Numerical Model of Activation of Liquid Water in Ice Clouds

The process of cloud phase transformation in an adiabatic parcel can be described by a system of the following equations.

The pressure variation equation:

$$\frac{dP}{dt} = -\frac{gpu_z}{R_aT}; \quad \text{(F1)}$$

the energy conservation equation:

$$\frac{dT}{dt} = -\frac{gu_z}{c_p} + \frac{L_w}{(1+q_v)c_p}\frac{dq_w}{dt} + \frac{L_i}{(1+q_v)c_p}\frac{dq_i}{dt}; \quad \text{(F2)}$$

the water mass conservation equation:

$$\frac{dq_v}{dt} + \frac{dq_w}{dt} + \frac{dq_i}{dt} = 0; \quad \text{(F3)}$$

the rate of change of the liquid droplets mass:

$$\frac{dq_w}{dt} = \frac{4\pi\rho_w}{\rho_a} A_w N_w r_w S_w; \quad \text{(F4)}$$

the rate of change of the ice particles mass:

$$\frac{dq_i}{dt} = \frac{4\pi c\rho_i}{\rho_a} A_i n_i r_i S_i; \quad \text{(F5)}$$

the rate of change of droplet size:

$$\frac{dr_w}{dt} = \frac{A_w S_w}{r_w}; \quad \text{(F6)}$$

the rate of change of ice particle size:

$$\frac{dr_i}{dt} = \frac{cA_i S_i}{r_i}. \quad \text{(F7)}$$

The explanation for the symbols is provided in appendix A. For $k(T)$, $L_w(T)$, and L_i(T) the dependence on temperature was taken into account. For $D(T, P)$ both temperature and pressure were considered. The ice particles in the above model were assumed to be spheres, having initial size $r_i(t_0) = 1$ μm. Both droplets and ice particles were assumed to have monodisperse size distributions. For supersaturation $S_w < 0$ liquid droplets were not allowed evaporate below $r_{\min} = 0.25$ μm. The capacitance of ice particles c during modeling was assumed to be constant and equal either to 1 or 0.5. The values of c in each specific case are indicated in the figure captions.

REFERENCES

Bergeron, T., 1935: On the physics of clouds and precipitation. *Proces Verbaux de l'Association de Météorologie,* Lisbon, Portugal, International Union of Geodesy and Geophysics, 156–178.

Borovikov, A. M., I. I. Gaivoronskii, E. G. Zak, V. V. Kostarev, I. P. Mazin, V. E. Minervin, A. K. Khrgian, and S. M. Shmeter, 1963: *Cloud Physics*. Israel Program of Scientific Translations, 393 pp.

Field, P. R., R. J. Hogan, P. R. A. Brown, A. J. Illingworth, T. W. Choularton, P. H. Kaye, E. Hirst, and R. Greenaway, 2004: Simultaneous radar and aircraft observations of mixed-phase cloud at the 100-m-scale. *Quart. J. Roy. Meteor. Soc.,* **130,** 1877–1904.

Findeisen, W., 1938: Kolloid-meteorologische Vorgänge bei Neiderschlags-bildung. *Meteor. Z.,* **55,** 121–133.

Fleishauer, R. P., V. E. Larson, and T. H. Vonder Haar, 2002: Observed microphysical structure of midlevel, mixed-phase clouds. *J. Atmos. Sci.,* **59,** 1779–1804.

Harrington, J. Y., and P. Q. Olsson, 2001: On the potential influence of ice nuclei on surface-forced marine stratocumulus cloud dynamics. *J. Geophys. Res.,* **106,** 27 473–27 484.

——, T. Reisin, W. R. Cotton, and S. M. Kreidenweis, 1999: Cloud resolving simulation of Arctic stratus. Part II: Transition-season clouds. *Atmos. Res.,* **51,** 45–75.

Heymsfield, A. J., 1977: Precipitation development in stratiform ice clouds—Microphysical and dynamical study. *J. Atmos. Sci.,* **34,** 367–381.

Illingworth, A. J., and Coauthors, 2007: Cloudnet—Continuous evaluation of cloud profiles in seven operational models using ground-based observations. *Bull. Amer. Meteor. Soc.,* **88,** 883–898.

Korolev, A. V., and G. A. Isaac, 2003: Phase transformation in mixed-phase clouds. *Quart. J. Roy. Meteor. Soc.,* **129,** 19–38.

——, and I. P. Mazin, 2003: Supersaturation of water vapor in clouds. *J. Atmos. Sci.,* **60,** 2957–2974.

——, G. A. Isaac, S. G. Cober, J. W. Strapp, and J. Hallett, 2003: Observation of the microstructure of mixed-phase clouds. *Quart. J. Roy. Meteor. Soc.,* **129,** 39–66.

Mazin, I. P., 1986: Relation of clouds phase structure to vertical motion. *Sov. Meteor. Hydrol.,* **N11,** 27–35.

Pinto, J. O., 1998: Autumnal mixed-phase cloudy boundary layers in the Arctic. *J. Atmos. Sci.,* **55,** 2016–2038.

Pruppacher, H. R., and J. D. Klett, 1997: *Microphysics of Clouds and Precipitation*. Kluwer Academic, 954 pp.

Rauber, R. M., and A. Tokay, 1991: An explanation for the existence of supercooled water at the top of cold clouds. *J. Atmos. Sci.,* **48,** 1005–1023.

Rodean, H. C., 1996: *Stochastic Lagrangian Models of Turbulent Diffusion*. *Meteor. Monogr.,* No. 48, Amer. Meteor. Soc., 84 pp.

Sedunov, Yu. S., 1974: *Physics of Drop Formation in the Atmosphere.* John Wiley & Sons, 234 pp.

Squires, P., 1952: The growth of cloud drops by condensation. *Aust. J. Sci. Res.,* **5,** 66–86.

Tremblay, A., A. Glazer, and W. Yu. R. Benoit, 1996: A mixed-phase cloud scheme based on a single prognostic equation. *Tellus,* **48,** 483–500.

Verlinde, J., and Coauthors, 2007: The Mixed-Phase Arctic Cloud Experiment. *Bull. Amer. Meteor. Soc.,* **88,** 205–221.

Wegener, A., 1911: *Thermodynamik der Atmosphäre*. J. A. Barth Verlag, 311 pp.

Wilson, D. R., and S. P. Ballard, 1999: A microphysically based precipitation scheme for the UK Meteorological Office Unified Model. *Quart. J. Roy. Meteor. Soc.,* **125,** 1607–1636.

Zawadzki, I., W. Szyrmer, and S. Laroche, 2000: Diagnostic of supercooled clouds from single-Doppler observations in regions of radar-detectable snow. *J. Appl. Meteor.,* **39,** 1041–1058.